

Near-keV Coherent X-Ray Generation with Sub-10-fs Lasers

Christian Spielmann, Clarence Kan, Neal H. Burnett, Thomas Brabec, Michael Geissler,
Armin Scrinzi, Matthias Schnürer, and Ferenc Krausz, *Member, IEEE*

(Invited Paper)

Abstract—Recent advances in solid-state laser technology and ultrafast optics have led to the generation of optical pulses as short as 5 fs with peak powers up to 0.1 TW from a compact kilohertz-repetition-rate all-solid-state laser. This source significantly pushes the frontiers of nonlinear optics. Intriguing possibilities include the development of a compact laser-driven coherent soft-X-ray source at photon energies near 1 keV, and the generation of attosecond XUV pulses. This paper analyzes strong-field ionization and high-harmonic generation in the few-cycle regime, and reviews the first experimental realization of high-harmonic generation with 5-fs pulses. These experiments have resulted in the emission of coherent X-rays at photon energies greater than 0.5 keV ($\lambda < 2.5$ nm), representing the highest photon energies achieved with a laser-driven coherent source so far. The generated XUV beam is well collimated and predicted to be delivered, after suitable spectral filtering, in a single burst of attosecond duration.

Index Terms—Atomic physics, nonlinear optics, nonlinear wave propagation, tunneling, ultrafast optics.

I. INTRODUCTION

THE UTILITY of ultrashort optical pulses originates mainly from their short duration and the fact that high-peak powers can be achieved with moderate pulse energies. Time-resolved spectroscopy is one of the “classic” application fields in which the short pulse duration is of prime importance. In nonlinear optics, the peak intensity has been appreciated as the key parameter with the shortness of the pulse regarded as necessary only to an extent which is needed to achieve the required peak powers. The possibility of “switching on” electric field strengths comparable to or higher than the atomic Coulomb field within a time comparable to the light oscillation cycle, which has now emerged with the development of a multigigawatt 5-fs laser source [1], promises to dramatically extend the frontiers of nonlinear optics and time-resolved spectroscopy. This extension relates to our ability to expose matter in its ground state to unprecedented field strengths. The implications are far reaching with respect to both fundamental aspects and applications. These include (but are not limited

to) the feasibility of above-barrier ionization, the generation of coherent X-rays from a laboratory source in the wavelength range between the oxygen and carbon K edge (2.3–4.4 nm), the so-called water-window, and the generation of single attosecond XUV pulses.

A bright laboratory X-ray source in the water-window is expected to have great impacts on biophysics and biochemistry, allowing the study of biological samples in their natural environment with high contrast and resolution. This research previously relied on the use of synchrotron radiation [2] or an X-ray laser pumped by a multikilojoule laser [3], both available at large-scale facilities only. Recently laboratory sources of coherent X-rays in the water window have been demonstrated by Spielmann *et al.* [4] and Chang *et al.* [5] by means of high-harmonic generation in helium. The use of sub-10-fs near-infrared (NIR) pump pulses limits the effective interaction time relevant for the generation of the highest harmonics to essentially one optical cycle, which, in combination with propagation effects, can result in the emission of a *single* attosecond X-ray pulse near the cutoff of the emitted XUV spectrum, as recently predicted by Kan *et al.* [6]. These extraordinarily short pulses are likely to open the way to the “atomic time scale” characterization of the quantum-mechanical evolution of the electron wave function in bound atomic states as well as for electronic processes in chemical reactions. Furthermore, the concentration of the X-rays within an extremely short time interval and the high degree of spatial coherence of the sub-10-fs laser-driven XUV source give rise to an unprecedented peak brightness, which paves the way toward an extension of nonlinear optics into the X-ray regime.

In this paper, we shall review the new possibilities sub-10-fs pump pulses open up in the research and development of compact laser-driven ultrafast coherent X-ray sources. The remaining part of this section is devoted, after a brief overview of recent advances in the technology of short-pulse lasers, to the physical processes relevant to short-wavelength generation and to a discussion of various routes to coherent X-ray generation. In the subsequent sections we shall focus on one of the most promising routes, high-harmonic generation, and the underlying physical processes.

Ultrafast solid-state laser technology has been subject to dramatic advances over the last 10 years. The invention of titanium-doped sapphire (Ti:sapphire) [7] along with the development of Kerr-lens mode-locking [8], [83], [84] and chirped

Manuscript received November 13, 1997; revised March 12, 1998. This work was supported by the Austrian Science Foundation under Grant Y44-PHY. The work of C. Spielmann was supported by an APART Fellowship.

C. Spielmann, T. Brabec, M. Geissler, A. Scrinzi, M. Schnürer, and F. Krausz are with Abteilung Quantenelektronik und Lasertechnik, Technische Universität Wien, A-1040 Vienna, Austria.

C. Kan and N. H. Burnett are with the Department of Electrical Engineering, University of Alberta, Edmonton, AB, T6G2G7 Canada.

Publisher Item Identifier S 1077-260X(98)03840-4.

dielectric mirrors for ultrabroad-band dispersion control [9] have resulted in a new generation of compact solid-state ultrafast oscillators, which can now routinely generate pulses in the sub-10-fs regime [10] with peak powers exceeding 1 MW [11], [85] and pulse durations as short as 6.5 fs [12]. Amplification of ultrashort pulses has also progressed rapidly. The combination of the technique of chirped pulse amplification [13] with Ti:sapphire allowed the construction of laboratory-scale high-power laser systems with unprecedented characteristics [1], [14]–[27]. Pulses as short as ≈ 20 fs have now become available with terawatt peak powers (pulse energy on the order of 100 mJ) at repetition rates of 10–50 Hz [22], [25]. The development of powerful kilohertz repetition rate pump lasers and the excellent thermal properties of Ti:sapphire opened the way to producing millijoule-energy 20-fs pulses at kilohertz frequencies [1], [27]. The output of these systems can now be spectrally broadened in a gas-filled capillary and subsequently compressed [28] at pulse energy levels many orders of magnitude higher than applicable in single-mode-fiber (SMF) compressors [29]. Using this technique (dubbed as the hollow-fiber technique), self-phase-modulated 20-fs pulses with energies of tens of microjoules have been compressed in a delay line consisting of chirped mirrors and fused-silica prisms to 4.5 fs [30], [86]. The more recent development of chirped mirrors providing proper dispersion control for self-phase modulated (SPM) pulses over a bandwidth of 150 THz (650–950 nm) [31] without relying on additional dispersive components has permitted upscaling the hollow-fiber-chirped-mirror compression technique to the submillijoule level while preserving the 5-fs duration [1], [32]. The electric field performs less than two oscillations within the full-width at half maximum (FWHM) of the intensity envelope of these pulses. They are delivered in a diffraction-limited beam and hence focusable to peak intensities in excess of 10^{17} W/cm².

The availability of light pulses comprising just a few oscillation cycles at intensities well above 10^{14} W/cm² opens up new prospects for nonperturbative nonlinear optics and coherent short-wavelength generation. Matter irradiated at these intensity levels undergoes tunnel ionization [33]–[35]. For pulses containing many oscillations, the number of ionized particles (e.g., atoms, molecules, or clusters) accumulates over many optical cycles, which may result in a depletion of the ground state well before the peak of the incident pulse impinges upon the target. Fig. 1(a) depicts the instantaneous ionization rate, as obtained from the theory of Ammosov, Delone, and Krainov (ADK) [34], [87]¹ induced in helium by the linearly polarized electric field of a 50-fs near-infrared (800 nm) laser pulse with a peak intensity of 4×10^{15} W/cm². Fig. 1(b) shows the ionization rate under the same experimental conditions except that the pulse duration is 5 fs. Fig. 1(b) also depicts the ionization rate for circular polarization (dashed line). The consequences of the dramatically shortened exposure to the laser field are numerous and far reaching. First, the peak electron emission (or ionization) rate is much higher than in the multicycle regime and can considerably exceed the laser frequency ($\approx 3 \times 10^{14}$ s⁻¹). Secondly, the freed electrons are

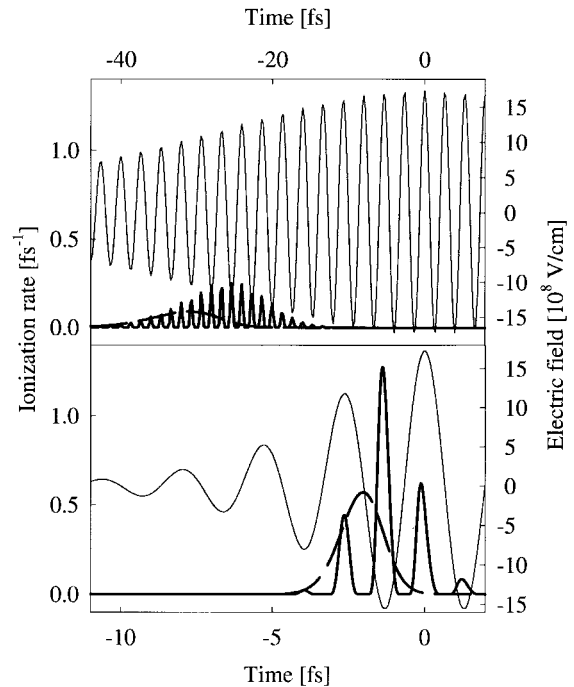


Fig. 1. (top) Instantaneous ionization rate induced in helium by a linearly (full line) or circularly (dashed line) polarized electric field (thin line) of a 50-fs NIR (800 nm) laser pulse with a peak intensity of 4×10^{15} W/cm². (bottom) Ionization rate under the same experimental conditions except that the pulse duration is 5 fs.

released into significantly stronger fields as compared to the multicycle regime. These implications suggest that coherent XUV generation resulting from a free-bound transition (high-order harmonic or continuum generation, henceforth, briefly HHG) [36], [37] will exhibit improved efficiency and generate higher XUV frequencies. In addition, electron-excited X-ray laser schemes (EEXL) [38], [39], [88] are likely to benefit from the improved energy coupling efficiency into an optically ionized plasma because the required high intensities can be achieved at much lower energy levels in the single cycle regime.

After ionization, the freed electron gains energy in the laser field. This is an essential process, because emission of high-energy photons is the result of the interaction of these electrons either with their parent ions (HHG) or with the surrounding ions in the ensemble (EEXL) in these schemes and the photon energy is limited by that of the recombining (HHG) or colliding (EEXL) electrons. Following Corkum *et al.* [40], [41], the electron motion in the laser field can be described by classical mechanics after tunneling. Fig. 2 shows electron trajectories for different polarization states of the laser field (linear and circular) and different release times t_r with respect to the phase of the electric field during the first laser period following ionization. The laser intensity was chosen as 4×10^{15} W/cm².

The electron reencounters its parent ion if and only if the laser field is linearly polarized and the electron is released at a suitable phase ωt_r of the laser field. The full line in Fig. 2 depicts the trajectory of the electron released at $\omega t_r = 17^\circ$, which was previously shown to yield the electron passing the nucleus

¹For hydrogen, the same expression was first obtained by [87].

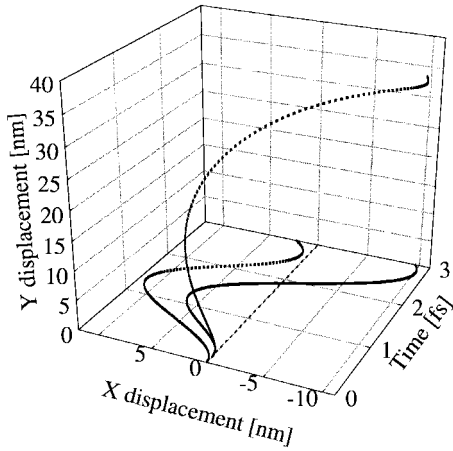


Fig. 2. Trajectories of the electron wavepacket in an electric field $E = E_0 \cos(\omega t)$ as a function of the time of ionization t_0 and polarization. The driving field has a cycle-averaged intensity of 4×10^{15} W/cm² and an oscillation period of 2.67 fs. An electron born at the field maximum (dotted line) will return to its parent ion with zero energy in a linearly polarized field. The electron born at $\omega t_r \approx 17^\circ$ (full line) will reencounter the parent ion with the maximum energy and give rise to the emission of the highest XUV photon energies emitted by upon recombination into the ground state. An electron born at any time will never recombine with his parent ion in a circularly polarized field (dashed), but it can gain a much higher drift energy, which may be beneficial for collisional excitation of neighboring atoms.

with maximum kinetic energy, given by $(W_{\text{kin}})_{\text{max}} \approx 3.17 U_p$ [41], [42], where U_p is the ponderomotive energy. In units of electronvolts it can be expressed as $U_p = 9.3 \times 10^{-14} I \lambda^2$, where I is the laser intensity and λ is the laser wavelength in units of W/cm² and μm , respectively. With some small probability the returning electron recombines in its original ground state upon emitting a photon with an energy equal to the sum of the ionization potential I_p and the electron kinetic energy W_{kin} gained in the laser field. Because the electron wavepacket evolution is driven by a spatially coherent laser field, the emission of the high-energy XUV photons from the particles in the ensemble also occurs in a spatially coherent manner, leading to a well-collimated XUV-beam collinear with the pump laser beam. In the multicycle regime, the process is repeated quasi-periodically over many laser periods, consequently the XUV emission spectrum is made up of discrete harmonics of the laser frequency. In the photon energy range close to the highest harmonics (cutoff region) the emission period has been predicted to be confined to a small fraction of the laser oscillation cycle. This prediction implies that the temporal evolution of the XUV output in the cutoff region can be characterized as a train of bursts of subfemtosecond duration [43]–[46]. It is obvious from the above considerations that the use of a quasi-single-cycle driver benefits HHG in several respects. First, higher photon energies (shorter wavelengths) can be achieved because the electrons are released into a stronger laser field (see Fig. 1). Second, The X-rays near cutoff can be emitted in a *single* attosecond pulse, resulting in an unprecedented concentration of electromagnetic energy. Third, efficiency is increased due to the higher ionization rate and an increased coherence length [6]. These benefits will be discussed in more detail in Section III.

For circularly polarized light, the electron never returns to its parent ion [41] (see, e.g., the trajectory depicted by the dashed line in Fig. 2). However, the average kinetic energy of the electrons associated with the drift (nonoscillating) component of their motion, which the electrons are left behind with after the laser field is off, can be far higher than for linearly polarized laser field. The average electron energy in the plasma produced by circularly polarized light is $(W_{\text{kin}})_{\text{av}} \approx U_p$ and the energetic electrons can serve as an efficient pump source for X-ray lasers as proposed by Burnett and Corkum [47]. For instance, they can induce bound–bound transitions of the electron system of the ions via collisions [38], [39], [88] and thereby generate population inversion for X-ray lasing. After multiple ionization, the transition energies fall into the soft X-ray region. This EEXL scheme has been successfully demonstrated in Xe⁹⁺ produced by a circularly polarized 40-fs laser focused to intensities of $\approx 3 \times 10^{16}$ W/cm² (XUV emission wavelength ≈ 42 nm, photon energy ≈ 30 eV) [38], [88]. Recent theoretical studies suggest that electron-excited X-ray lasers could be scalable to photon energies approaching [48] or even exceeding [39] 1 keV.

Yet another route to coherent X-ray generation that opens up with the availability of few-cycle drivers is high-harmonic generation in crystalline solids. Recently Kalman and Brabec [49], [50] proposed a scheme which should allow the generation of coherent kiloelectronvolt X-rays by the use of very short pump pulses. Their approach draws on the idea that for sufficiently short pulse durations high intensity can be coupled into a crystal before the lattice structure is destroyed. The periodic potential of the crystal lattice is important for two reasons. First, the X-ray generation is enhanced by an additional momentum transfer from the lattice. Second, via Bragg coupling the X-ray modes with the minimum absorption losses are selected. These two effects will lead to substantial decrease of the threshold pump laser intensity required for kilohertz X-ray generation as compared to free electrons. For a successful realization of this scheme it is crucial that the pump pulses are much shorter than the electron–phonon relaxation time which is on the order of 100 fs. Numerical simulations have shown that focusing sub-30-fs pulses with a peak intensity of 10^{17} W/cm² onto a LiF crystal will result in the emission of coherent X-rays with photon energies of ≈ 3 keV having a brilliance comparable with synchrotron radiation [49].

The above examples demonstrate the tremendous potential for coherent X-ray generation that can be exploited with powerful ultrashort light pulses in the few-cycle regime. The new ultrafast drivers hold promise for both improving existing techniques significantly and for opening new ways to producing high-energy X-rays with laboratory sources. Furthermore, they also permit operation of laser-driven X-ray sources at laser pulse energies far smaller than in the multicycle regime. The relaxed pump energy requirements do not only allow the use of more compact laser drivers but also pave the way to significantly higher repetition rates, implications carrying much weight when it comes to applications of the novel X-ray sources.

The remaining part of this paper is organized as follows. Section II is devoted to strong-field ionization, the primary

physical process in all high-field laser-atom interactions. For pulses consisting of many cycles and intensities significantly greater than 10^{14} W/cm², ionization occurs in the optical tunneling regime and is essentially completed in this same regime because the ground state is depleted before the laser field could become strong enough to suppress the Coulomb barrier below the ionization potential (in helium this occurs at an electric field of $E_{bs} \approx 10^9$ V/cm). As a consequence, ionization can be accurately described by the analytic theory of optical tunnel ionization [33]–[35]. Fig. 1(b) clearly reveals that the ground state remains populated up to electric fields well beyond E_{bs} in the single-cycle regime. Therefore, the validity of the widely used analytic expressions in this previously inaccessible regime is brought into question. In Section II predictions of the analytic ADK theory is compared with results obtained by numerically solving the time-dependent Schrödinger equation for hydrogenlike atoms in the presence of a strong laser field. Sections III and IV focus on the theory of HHG and its experimental realization in the quasi-single-cycle regime (XUV continuum generation). In Section III, we analyze the XUV emission of helium resulting from a (quasi-)free-bound transition induced by ultrashort laser pulses in the few-cycle regime. The analysis is not confined to an isolated atom, but also performed for an ensemble by using a quasi-classical description [41], [51] and the Maxwell equation for describing propagation of the pump and XUV wave. The XUV output is compared for different pump pulse durations. In Section IV, we review recent HHG experiments which were carried out with sub-10-fs pulses [4], [52]. The presented source emits an XUV continuum with excellent spatial coherence. Coherent XUV generation in the range of several hundred eV (extending beyond 0.5 keV) has been demonstrated for the first time at a kilohertz repetition rate in these experiments. Section V summarizes the challenges left to be addressed for the generation, control, and measurement of single attosecond XUV pulses and their use for spectroscopy and nonlinear optics.

II. STRONG-FIELD IONIZATION IN THE FEW-CYCLE REGIME

Ionization is of prime importance being the first step in high-intensity light-matter interaction processes. Ionization, acceleration by the electric field, and subsequent collision of the electron with its parent ion or with adjacent atoms is responsible for number of exciting phenomena in strong-field atomic, plasma, and solid-state physics, including beyond HHG and X-ray lasing, laser-induced damage of dielectrics [53], [54], molecular dissociation [55], [56], plasma heating [57], etc. The theoretical investigation of the above processes is simplified tremendously by the analytical description of ionization. This has been possible in two parameter ranges defined by $\gamma \gg 1$ and $\gamma \ll 1$, where γ is the Keldysh parameter [33]. It is defined as $\gamma = \omega_0/\sqrt{2m_e I_p}/eE$, where e is the electron charge, m_e is the electron mass, I_p is the ionization potential, and E is the amplitude of the oscillating electric field. If $\gamma \gg 1$, ionization can be described perturbatively in the regime of multiphoton ionization. The opposite limiting case is characterized by $\gamma \ll 1$, where ionization takes place

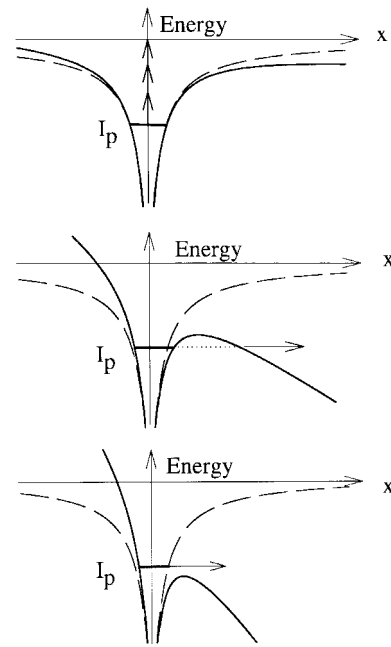


Fig. 3. Regimes of strong-field ionization. Exposing an atom to an intense laser field will result in a modified potential (solid line) composed of the Coulomb potential (dashed line) and the time dependent effective potential of the optical pulse. At moderate intensities the resulting potential is close to the unperturbed Coulomb potential and an electron can be liberated only upon simultaneous absorption of N photons, resulting in (*perturbative*) multiphoton ionization. The multiphoton ionization rate scales with the N th power of the intensity of the optical pulse. At sufficiently high-field strengths the Coulomb barrier becomes narrow, allowing optical tunnel ionization to take over and resulting in a tunneling current that follows adiabatically the variation of the resultant potential. At very high fields, the electric field amplitude reaches values sufficient to suppress the Coulomb barrier below the energy level of the ground state, opening the way to above-barrier ionization.

as a result of tunneling [33], [34], [87]. The limiting cases of multiphoton ionization (at moderate intensities) and tunnel ionization (at high intensities) are illustrated schematically in Fig. 3(a) and (b). Tunneling takes over for $\gamma \leq 1/2$, which is fulfilled for neutral atoms at intensities ranging from 10^{14} W/cm² to 10^{15} W/cm² in the near infrared spectral range. In strong field experiments preferably noble gases are used because of their chemical inactivity. A typical representative is helium (having the highest ionization potential, $I_p = 24.6$ eV) for which $\gamma < 1/2$ at a wavelength of 800 nm calls for an intensity of $I > 8 \times 10^{14}$ W/cm².

As the duration of intense laser pulses approaches the light oscillation period, a new regime of ionization comes into play. Because the peak electric field in these pulse are “switched on” virtually abruptly, a significant fraction of the ground-state population survives until the electric field reaches the barrier-suppression limit, i.e., the Coulomb barrier in the direction of the electric field is suppressed below the ionization potential and the bound electron can escape freely, as illustrated in Fig. 3(c).

The critical field strength at which this phenomenon occurs in a hydrogen-like atom is given in atomic units (1 a.u. = 5.14×10^9 V/cm) by $E_{bs} = I_p^2/(4Z)$, where Z is the charge of the residual ion and I_p is the ionization potential in atomic units (1 a.u. = 27.21 eV) [58]. The amplitude of the optical field is related to the (cycle-averaged) intensity in SI units

by $I[\text{W}/\text{cm}^2] = |E[\text{V}/\text{cm}]|^2/(2Z_0)$, where $Z_0 = 377 \Omega$. Applying these simple formulas to He ($Z = 1$, $I_p = 24.6$ eV), the intensity needed for barrier suppression, also referred to as the appearance intensity, is $I_{ap} \approx 1.5 \times 10^{15} \text{ W}/\text{cm}^2$. Fig. 1(b) reveals that according to the optical tunneling rate [33]–[35], which was used for calculating the ionization dynamics depicted in Fig. 1, a dominant fraction of the helium atoms irradiated by a 5-fs pulse at $\lambda_0 = 800$ nm is ionized at field strengths greater than E_{bs} . This prompts the question if the optical tunnel rate [33]–[35] gives proper account for strong-field ionization in the quasi-single-cycle regime.

In what follows, we will investigate ionization numerically in the parameter range of above-barrier ionization and compare the results with the predictions of the analytic theory of optical tunnel ionization. For $\gamma \leq 1/2$, it was shown (see ADK-rate [34], [87] and the Keldysh-rate [33] corrected for the effect of the Coulomb potential by Krainov [35]) that optical tunneling can be described by DC tunneling [59], [60] with the dc electric field being replaced by the fast oscillating laser electric field. The ADK-theory [34], [87] as well as the Keldysh theory [33] after Coulomb correction [35] yield the following expression for the rate of optical tunnel ionization from the ground state

$$w(t) = \omega_p |C_{n^*}|^2 \left(\frac{4\omega_p}{\omega_t} \right)^{2n^*-1} \exp \left(-\frac{4\omega_p}{3\omega_t} \right) \quad (1)$$

with

$$\begin{aligned} \omega_p &= \frac{I_p}{\hbar} \\ \omega_t &= \frac{eE_l(t)}{(2mI_p)^{1/2}} \\ n^* &= Z \left(\frac{I_{ph}}{I_p} \right)^{1/2} \\ |C_{n^*}|^2 &= 2^{2n^*} [n^* \Gamma(n^* + 1) \Gamma(n^*)]^{-1}. \end{aligned}$$

Here, I_p is the ionization potential of the species of interest, I_{ph} is the ionization potential of the hydrogen atom, and $E_l(t)$ is the electric field of the laser pulse. From the ionization rate $w(t)$, the density of freed electrons $n(t)$ can be obtained by solving a simple rate equation, yielding

$$\frac{n(t)}{n_0} = 1 - \exp \left[-\int_{-\infty}^t dt' w(t') \right] \quad (2)$$

where n_0 is the density of atoms.

The process of ionization can also be studied by solving numerically the time-dependent Schrödinger equation. The numerical solver is based on the complex scaling method. The wave equation is expanded in Laguerre polynomials, where the equations governing the time dependent amplitudes are solved by a Runge–Kutta scheme. The free electron density left behind by the pulse is then given by $n_f = n_0(1 - |\psi|_b^2)$, where $|\psi|_b^2$ denotes the projection of the wavefunction onto the bound states of the atom. Computer simulations have been carried out for hydrogen in the presence of a strong laser pulse for different pulse durations in the few-cycle regime. The results of this study are summarized in Fig. 4, which plots

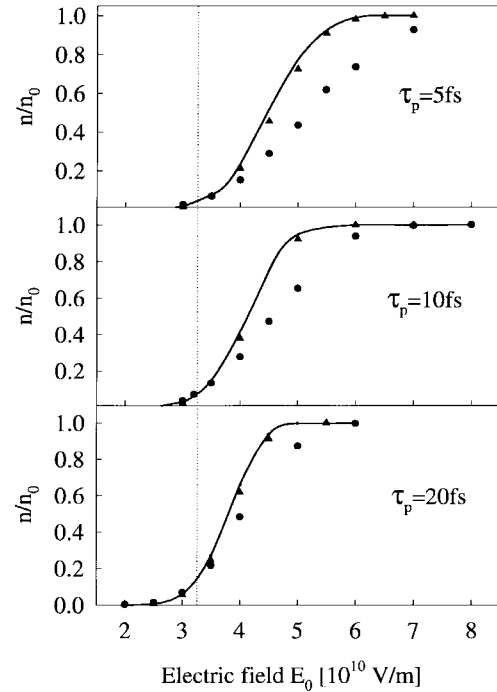


Fig. 4. Fraction of ionized hydrogen atoms in the regime of above-barrier ionization as function of the peak electric field amplitude for pulses of 5, 10, and 20 fs in duration. The full line shows the prediction of the ADK model, the triangles represent that of the Krainov model and the circles depict the exact solution of time-dependent Schrödinger equation. The dotted line depicts the barrier suppression field strength for hydrogen ($E_{bs} \approx 3.2 \times 10^8$ V/cm).

n_f/n_0 as a function of the peak electric field strength E_0 for different pulse durations.

The full lines depict the results obtained by using the ADK-rate [34], [87] whereas the triangles represent the prediction of the theory of Krainov [35], who extended the tunneling theory into the barrier suppression regime. The dots show the results gained from the exact numerical solution of the Schrödinger equation. The appearance intensity for a hydrogen atom is given by $I_{ap} = 1.4 \times 10^{14} \text{ W}/\text{cm}^2$ and the corresponding electric field amplitude is indicated by the dotted line in Fig. 4. It is interesting that little difference is found between the barrier-suppression rate of Krainov and the tunneling rate of ADK even well above E_{bs} . However, we find that the analytic results increasingly deviate from the exact solutions for decreasing pulse durations for $E_0 > E_{bs}$. This is because, for shorter pulse durations a larger fraction of the electrons is ionized at intensities falling into the barrier suppression regime. Nevertheless, even at high intensities and close to the single-cycle regime ($\tau_p = 5$ fs) the predictions of the tunneling theory do not deviate from the exact calculations by more than a factor of 2. It is important to note that the analytic tunneling theory increasingly overestimates ionization as the pulse duration approaches the single-cycle regime. As a consequence, atoms can be exposed to intensities higher than predicted by the tunneling theory before the ground state is depleted. This finding is important for HHG, as will become apparent in the next section. For exact modeling of HHG from an atomic ensemble the coupled Schrödinger and Maxwell equations should be solved numerically. Because this

is excessively time-consuming, the tunneling theory is used in the following section to determine the ionization rate [6]. It should be kept in mind that the tunneling theory overestimates the ionization rate for quasi-single-cycle drivers. However, the quantitative error introduced in the modeling in this manner does not significantly change the qualitative behavior of the HHG process.

III. STRONG-FIELD-DRIVEN FREE-BOUND TRANSITION: HIGH-ORDER HARMONIC AND XUV CONTINUUM GENERATION

Coherent XUV emission through the process that has come to be understood as “ultrahigh-harmonic generation” has been studied for many years [61]. In this process, the XUV emission is thought to arise from the re-interaction of an essentially free electron wavepacket with its parent ion some fraction of an optical cycle after its appearance in the continuum [41], [42], [51]. The XUV emission is inextricably linked to the ionization event itself with the induced nonlinear polarization being proportional to the square root of the ionization rate. Coherent XUV emission can result from this interaction only if the coherence of the fundamental forces a large number of atoms to radiate in phase. The observed XUV emission is thus determined both by the individual atomic response and by the phase mismatch between the fundamental and harmonic fields. For very high-frequency emission such as we study here, the XUV field can be considered as propagating in vacuum (phase velocity c), the presence of free electrons however leads to a slight increase in the phase velocity of the fundamental. Time dependent ionization also leads to dispersion and self phase and amplitude modulation (SPAM) of the fundamental. These factors (the relative importance of which depends somewhat on pulse length) ultimately limit the coherent growth of the XUV emission. It is apparent that a phase advance of the fundamental of a fraction of a percent will interfere with the coherent growth of XUV whose frequency is more than one hundred times the fundamental frequency, i.e., very delicate distortions of the visible field will destroy the coherent growth of the high frequency XUV radiation.

Ultrashort (few-cycle) pulses offer several advantages in this process [45], [62]: First, the semiclassical picture predicts a cutoff in the harmonic spectrum at a harmonic energy corresponding to [41], [42]

$$(h\nu)_{\max} \approx I_p + 3.17U_p. \quad (3)$$

In a pulsed laser field, U_p is time-dependent and can be defined in terms of the instantaneous amplitude (envelope) of the electric field (which may not be strictly speaking correct in the few cycle regime). Note that for intense pump pulses U_p relevant to (3) may not be dictated by the peak intensity but the one at which the ground state is depleted on the leading edge of the pulse (see Fig. 1) [5]. For ultra-short pulses, ionization and the related XUV frequency conversion can persist to much higher intensities which allows coherent XUV generation at higher X-ray photon energies than is the case with longer pulses. Furthermore, the desired characteristics of a high nonlinear polarizability (high ionization rate) and a large coherence length (low level of ionization) appear on

the surface to force one in the direction of shorter pulses for optimum conversion efficiency. The onset of SPAM at very short pulse durations will ultimately set a limit to this trend (see discussion below). Finally as we will show here, sub-10-fs driver pulses offer the prospect of concentrating the high frequency XUV in a single ≈ 100 -as subpulse. Control of the phase of the fundamental will allow synchronization of this subpulse with external events and permit the achievement of previously impossible temporal precision in pump-probe experiments. We have examined numerically in the one-dimensional (1-D) limit these aspects of the high-frequency XUV conversion process. The main finding of our study is outlined in [6] and is the observation that for driver pulses as short as 5-fs SPAM does not interfere with the coherence growth of XUV emission for frequencies well beyond the carbon K-edge at 280 eV. In the present paper we present some additional results concerning the pulse length dependence of the coherent growth of high-frequency XUV emission. We observe that for a Ti:sapphire driver a pulse length in the vicinity of 5 fs is likely near optimum.

In what follows, we combine the model of the nonlinear polarization, developed by Lewenstein *et al.* [51] with ground state depletion based on the ADK tunnel ionization rate [34], [87] and a 1-D numerical solution of the Maxwell wave equation for the fundamental and harmonic fields. The 1-D aspect of this study limits its applicability, of course, to situations where the target is much thinner (a fraction of a percent) of the confocal parameter. In the experiments discussed in Section IV, this requirement is only marginally met, nevertheless we expect the 1-D model to be of some assistance in interpreting the results and planning future directions.

In the experiments, as described in the next section, the helium atoms were irradiated with intensities up to $4 \times 10^{15} \text{ W/cm}^2$, which is almost three times the appearance intensity. In Section II, it was shown that the ionization rate is overestimated by the ADK approach at such high intensities. To estimate the error in the radiation spectrum of an isolated atom that is caused by this overestimation, the prediction of the model of Lewenstein *et al.* [51] has been compared with the square of the Fourier spectrum of the expectation of the dipole acceleration obtained from the exact numerical solution of the time-dependent Schrödinger equation for hydrogen. The chosen peak intensity of $5 \times 10^{14} \text{ W/cm}^2$ of the 5-fs driver pulse ($\lambda_0 = 800 \text{ nm}$) exceeds by approximately a factor of 3 the appearance intensity. The results are shown in Fig. 5. The prediction of the model of Lewenstein *et al.* [51] is found to be in good qualitative agreement with the exact numerical solution of the Schrödinger equation. However, due to the ionization rate significantly overestimated by the ADK-formula at these intensity levels, the model overestimates the intensity of high-harmonic radiation by approximately an order of magnitude at high frequencies. In order to reduce this deviation, the following simulations describing collective HHG in a helium ensemble are restricted to a peak pulse intensity of $2 \times 10^{15} \text{ W/cm}^2$, which only moderately exceed the appearance intensity.

To calculate HHG in an atomic ensemble, we first solve numerically the 1-D Maxwell wave equation for the driver

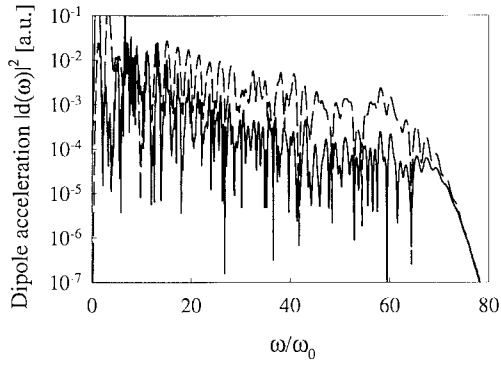


Fig. 5. Square of the dipole acceleration spectrum of a hydrogen atom exposed to a 5-fs pulse carried at $\lambda_0 = 800$ nm and having a peak intensity three times higher than the appearance intensity. The full line depicts the exact solution of the time dependent Schrödinger equation. The dashed line shows the prediction of the model of Lewenstein *et al.* combined with the ADK depletion of the ground state.

field in the presence of field dependent ionization as given by the ADK formula. This solution is used to compute the nonlinear polarization of the medium using the model of Lewenstein *et al.* and then finally the XUV emission is obtained by solving the wave equation with the induced nonlinear polarization as a source. In this final step, an approximate solution for the high frequency field is used where we neglect the influence of free electrons on propagation. This is justifiable since we are interested only in XUV frequencies for which $n/n_c \ll 1$, where n_c is the critical density.

First, we decompose the laser electric field in envelope and carrier

$$E_I(z, t) = A_I(z, t)e^{i(k_0 z - \omega_0 t + \psi_0)} + c.c. \quad (4)$$

This decomposition was shown to be physically meaningful down to pulse durations comparable to the carrier oscillation cycle $T_0 = 2\pi/\omega_0$ [63]. The Maxwell wave equation for the complex envelope $A_I(z, t)$ of the fundamental field in an ionizing medium can then be written as

$$\frac{\partial^2 A_I}{\partial z^2} - \frac{1}{c^2} \frac{\partial^2 A_I}{\partial t^2} + \frac{2i\omega_0}{c} \left(\frac{\partial A_I}{\partial z} + \frac{1}{c} \frac{\partial A_I}{\partial t} \right) - \frac{\omega_p^2(E_I, t)}{c^2} A_I = 0 \quad (5)$$

where $\omega_p^2(E_I, t) = 4\pi n(E_I, t)e^2/m_e$ is the square of the electron plasma frequency and $n(E_I, t)$ is given by (1) and (2). Solving the wave equation in envelope form besides affording some computational advantages provides direct access to phase and amplitude deviations of the fundamental from those corresponding to vacuum propagation. The solution for the fundamental field is then used to calculate the time and spatially dependent nonlinear polarization in the ionizing medium, which is subsequently inserted into the wave equation for the XUV electric field $E_h(z, t)$ neglecting dispersion, i.e.,

$$\frac{\partial^2 E_h}{\partial z^2} - \frac{1}{c^2} \frac{\partial^2 E_h}{\partial t^2} = \frac{4\pi}{c^2} n_0 d_a^h(E_I, t) \quad (6)$$

where d_a^h is the second time derivative of the atomic dipole moment, henceforth dipole acceleration, as calculated from the model of Lewenstein *et al.* [51]. This latter equation is

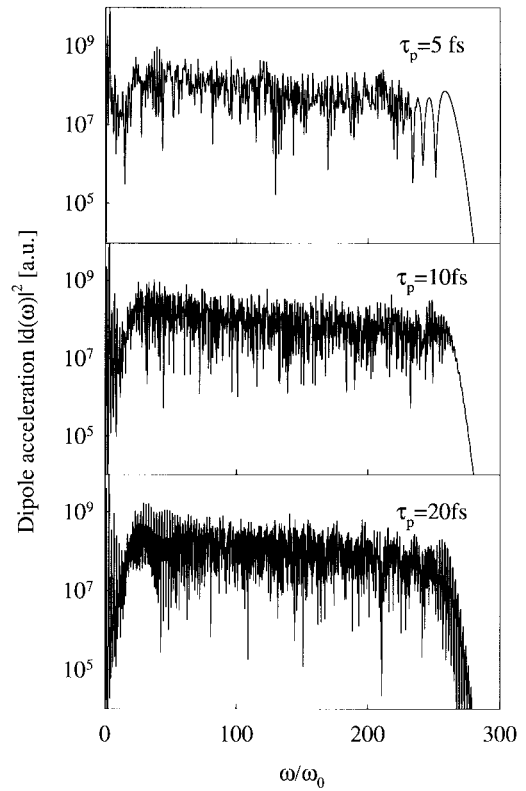


Fig. 6. Square of the dipole acceleration spectrum of helium exposed to laser pulses with a fixed peak intensity of 2×10^{15} W/cm² at $\lambda_0 = 0.8$ μ m for different pulse durations.

solved using a Fourier transform method [64]. The phase and amplitude of the numerically propagated fundamental is defined at the entrance ($z = 0$) to the medium (500-torr He) as $E_I(0, t) = A_I(0, t) \exp(-i\omega_0 t + i\psi_0)$, where $A_I(0, t)$ was taken as Gaussian peaking at $t = 0$. The relative phase between the carrier and its envelope (ψ_0) turns out to be a significant parameter in our calculations. In what follows, unless otherwise noted, we have chosen $\psi_0 = 0$, i.e., a “cosine pulse” where the field peaks at the peak of the envelope.

In Fig. 6, we show the square of the Fourier transformed dipole acceleration (single atom response) for He atoms exposed to pulses with a peak intensity of 2×10^{15} W/cm² and carrier wavelength 800 nm of varying temporal duration. Note that the discrete harmonic structure is entirely absent near cutoff for $\tau_p = 5$ fs, indicating that emission of these high-energy photons is confined to one optical cycle in this case. Fig. 7 depicts the fundamental waveform at the entrance to the medium, time dependent ionization fraction from the ADK formula, and the square of the envelope of the inverse transformed dipole acceleration after applying a spectral filter to isolate components of frequency ranging from 240–280 times the carrier frequency. This latter curve corresponds to the radiation intensity envelope that would be emitted by an isolated atom at $z = 0$. In Fig. 8 we show these same parameters after propagating through 10 μ m of the medium. In this case, we show the radiation intensity envelope of the forward propagating coherent XUV signal, again after a spectral filter applied to isolate components in the range h240–h280.

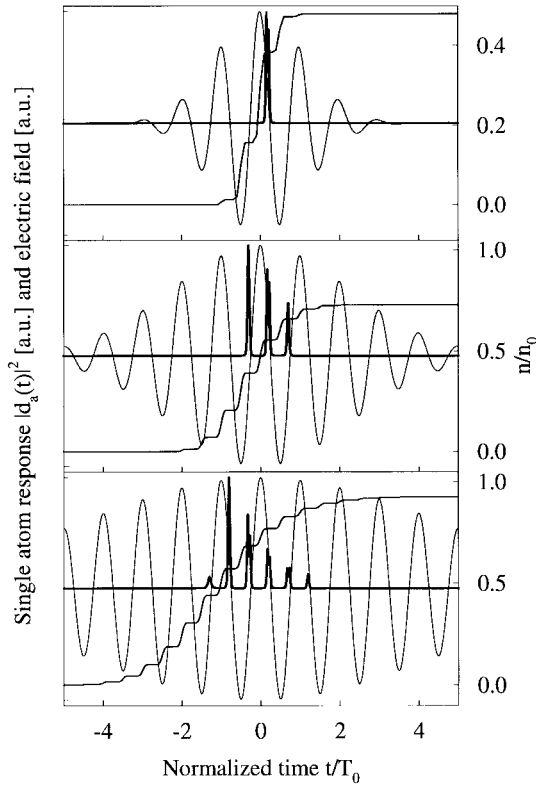


Fig. 7. Fundamental waveform, ionization profile and square of the dipole acceleration (single atom response) after applying a spectral filter to isolate components of frequency ranging from 240 to 280 times the carrier frequency for He atoms subjected to pulses of a peak intensity of 2×10^{15} W/cm² carried at $\lambda_0 = 800$ nm with different temporal duration. The scale for $|d_a(t)|^2$ is different for different pulse durations.

The number of 400-eV photons per unit area (full lines) and the peak intensity of the most intense micropulse (dotted lines) as a function of propagation distance are shown in Fig. 9 for pulse durations of 5, 10, and 20 fs. We have done a similar calculation for a 2.5 fs pulse, in this case the saturated peak intensity decreases to a value near that observed for the 10-fs case. We find that, in this latter case, self-phase and amplitude modulation (SPAM) and not simple free electron induced phase advance is the dominant limit to coherent growth. SPAM in a medium undergoing time dependent ionization leads to a frequency increase and amplitude reduction [65] of the fundamental which alters highest frequency XUV emission that is permitted by the $3.17 U_p$ cutoff rule, this also modifies the relative phase of the induced dipole moment at a given permitted XUV frequency. Fig. 9 indicates that 5-fs pulses are, owing to an enhanced coherence length, capable of generating by two orders of magnitude more 400-eV photons and three orders of magnitude higher peak intensities at these high-photon energies than 20-fs pulses. This is all the more remarkable when one considers that the comparison is made at constant peak powers, i.e., the energy of the 5-fs pulses is substantially lower as compared to the 20-fs pulses.

The micropulse structure seen in the XUV signal plotted in Figs. 7 and 8 is due to the nature of the classical trajectories of electrons which tunnel with small initial energy into an optical field. Electrons which re-encounter their parent ions with the highest energy are born in a narrow phase bin of

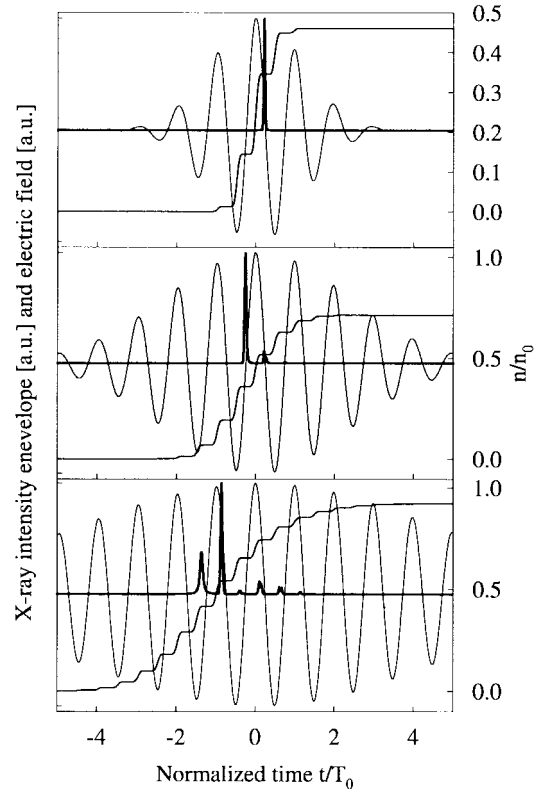


Fig. 8. Fundamental waveform, ionization profile and forward propagating radiation intensity after applying a spectral filter to isolate components of frequency ranging from 240 to 280 times the carrier frequency for He atoms subjected to pulses of peak intensity 2×10^{15} W/cm² and $\lambda_0 = 0.8$ μ m of varying temporal duration. The results were obtained after a propagation length of 10 μ m in 500-torr He. The scale for the XUV intensity is different for different pulse durations.

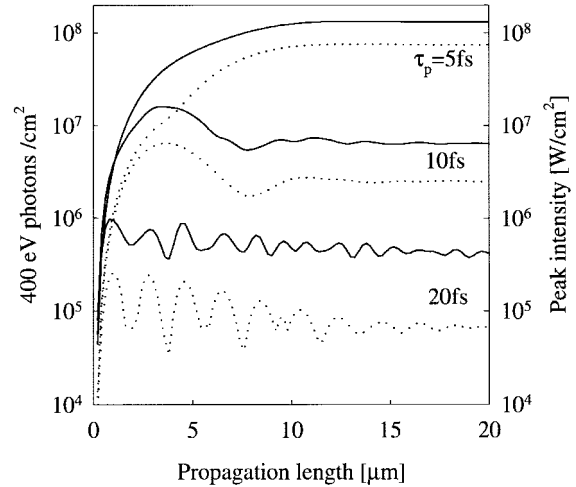


Fig. 9. Number of 400-eV photons per area within the filter band as given in Figs. 7 and 8 (solid lines) and peak intensity of the most intense micropulse (dotted lines) as a function of propagation distance for pulse durations of 5, 10, and 20 fs.

the fundamental just after ($\approx 17^\circ$) a peak in the fundamental field (see full line in Fig. 2) and return about 2/3 of a cycle later in a narrow bin near a zero crossing of the electric field [41], [43]. Depending on the spectral window employed to isolate the emission, individual micropulses can have durations

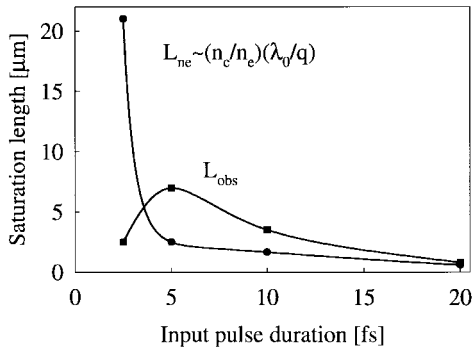


Fig. 10. Saturation length for the coherent growth of XUV radiation in the frequency range $240 < \omega/\omega_0 < 280$ as a function of the pulse duration for a fixed peak intensity of 2×10^{15} W/cm² in 500-torr He. The dots represent the “quasi-static” coherence length caused by ionization. The squares depict the computed coherence lengths as extracted from the results shown in Fig. 9.

considerably shorter than 100 as. In Fig. 9, we plot the peak intensity of the largest micropulse. The coherent growth of individual micropulses is roughly determined by the electron density that existed near the time when electrons responsible for that micropulse first appear in the continuum. So that generally the first micropulse that is allowed by the $3.17 U_p$ cutoff rule, seeing the lowest electron density, grows the most robustly.

Our calculations in regard to the pulselength dependence of the coherence length for growth of XUV emission in the frequency interval between h240 and h280 are summarized in Fig. 10. Here, we show the propagation length in 500-torr He over which the peak intensity of emission in this frequency interval grows to 90% of its saturated value as well as the expected coherence length L_{ne} for a plasma with electron density, n_e , corresponding to that existing when the electrons responsible for the most intense micropulse first appear in the continuum, i.e., $L_{ne} \approx n_c/n_e \lambda_0/q$ [66].² Here, n_c denotes the critical electron density at the fundamental laser carrier wavelength λ_0 and q denotes the “harmonic” order. Also plotted is the observed saturation length for the strongest micropulse from our propagation code. It is apparent that the limits to coherence for pulses longer than 20 fs can be thought of in terms of quasi-static plasma dispersion. For pulses in the range from 20–5 fs, the coherence length is improved, apparently as a consequence of the breakdown of the slowly varying envelope approximation [6]. Our results suggest that in the few-cycle regime the relevant velocity for phase matching is intermediate between the quasi-static phase velocity ($>c$) and the group velocity ($<c$). For pulselengths below 5 fs, the coherent growth of the XUV emission is limited by SPAM of the fundamental rather than by quasi-static plasma dispersion. It is apparent from Fig. 10 that the optimum pulse duration for efficient XUV emission is in the vicinity of 5 fs.

As is apparent from Fig. 8, this pulse duration has the coincidental benefit of allowing single-micropulse selection by means of simple spectral filtering. In practice both the XUV micropulse selectivity or contrast as well as the saturated peak

intensity of the strongest micropulse depend somewhat on the relative carrier phase chosen for our calculation. We will not elaborate on this point here except to note that, somewhat surprisingly, for a 5-fs envelope, $\psi_0 = 0$ is not the optimum phase for efficient coherent XUV production. Likewise the micropulse contrast after propagation can be optimized by varying the carrier phase. In this case, the optimum phase is observed to vary somewhat depending on the chosen spectral window.

Although care must be taken in applying the results of a 1-D analysis such as used here to frequency conversion with a focused laser beam, the concept of a definable carrier phase (relative to its envelope) will still apply to a focused beam in the limit that the target thickness is much less than the confocal parameter. As few-cycle lasers will eventually have multimillijoule pulse energies, experiments will eventually closely approach this 1-D regime. In this case it is clear from Fig. 9 that, providing the fundamental has something approaching a “top hat” intensity profile and geometric phase advance is negligible in the nonlinear medium, stable, single attosecond pulse selection is possible through simple spectral filtering with a 5-fs driver. Present generation solid state lasers emit a stable (soliton-like) amplitude envelope and frequency spectrum but the relative phase between carrier and envelope is in practice random [67]. Stable single attosecond pulse selection will require access to and control over this phase. We will return to this point in Section V.

IV. COHERENT XUV CONTINUUM GENERATION WITH SUB-10-fs LASER PULSES

The ultrashort-pulse laser driver used for the XUV generation experiments reviewed below is an all-solid-state Ti:sapphire-based oscillator-amplifier system followed by a hollow-fiber-chirped-mirror pulse compressor. The system is described in detail elsewhere [1], [32]. Briefly, the front end of the laser system is a 10-fs Ti:sapphire oscillator (FemtoSource Pro, FemtoLasers GmbH) pumped by a frequency-doubled, diode-pumped Nd:YVO₄ laser (Millennia, Spectra Physics Inc.). The oscillator routinely delivers sub-10-fs pulses with an energy of about 5 nJ. The pulses are nearly transform limited and have a spectral width of about 100 nm centered at 780 nm. After stretching the pulses to several ps by a 10-cm-long slab of SF57, the energy is boosted by almost six orders of magnitude in a confocal eight-pass amplifier. The amplifier is pumped with an energy of 10 mJ at a 1-kHz repetition rate provided by a continuous-wave (CW) lamp-pumped intracavity frequency-doubled Q-switched Nd:YLF laser (Model 621D, BMI). Owing to a simple amplified spontaneous emission (ASE) suppression scheme the amplifier delivers pulses with energies up to 1.5 mJ and an ASE-to-amplified-energy ratio as low as $<2 \times 10^{-3}$. The pulse-to-pulse energy fluctuations are 1% rms [1]. The amplified pulses are compressed by a pair of double-fused silica prisms. The throughput is about $\approx 90\%$. The residual high-order dispersion is compensated by a pair of mirrors which are placed in front of the amplifier. This allows to keep the throughput of the compressor at maximum. The

²For a discussion of the coherence length dictated by a quasi-static free-electron density see, e.g., [66]. The situation for the short pulses we consider here is somewhat more complicated and is discussed by C. Kan *et al.* [6].

compressed pulses have a duration of 20–25 fs and energy of typically 1.1–1.2 mJ. The performance of the stretcher and compressor is not alignment sensitive, therefore, these results are reproducible on a day-to-day basis without any time-consuming alignment.

Subsequently these pulses are coupled into a hollow waveguide filled with a noble gas. The gas acts as a nonlinear medium in which spectral broadening via self phase modulation takes place [28]. The best performance for the given input pulses was achieved with an argon-filled 85-cm-long fiber having an inner diameter of 260 μm . After passage through the fiber the 50-nm-wide input spectrum broadens to more than 200 nm and is slightly blue shifted. The blue shift may arise from self steepening and some plasma formation. The fiber serves not only as a nonlinear medium but also acts as a very efficient spatial filter. As a consequence the linearly polarized output beam is diffraction limited within 10% and has a nearly Gaussian far-field distribution. Finally, the pulses are compressed in a dispersive delay line consisting of chirped mirrors. They introduce a nearly constant group-delay dispersion (linear variation of the group delay) over a range of 650–950 nm. Five to seven bounces off these mirrors compensate the chirp induced by SPM and precompensate the material dispersion between compressor output and experimental target and result in pulse durations of typically 5–7 fs on target. The output pulse energy is 0.4–0.5 mJ, yielding peak powers up to ≈ 0.1 TW. Owing to the diffraction-limited nature of the beam [1], these intense kilohertz-rate 5-fs pulses can be focused to peak intensities well in excess of 10^{17} W/cm².

Special care has to be taken when employing 5-fs pulses in experiments, because the pulses broaden by almost a factor of three upon traveling a distance of 1 m in air. To ensure minimum pulse duration at the target, the dispersion of air (and of possible optical components) has to be precompensated. The right amount of compensation can be adjusted by setting up a reference path. In this reference path the pulses experience the same amount of dispersion (glass and air) before they are measured with an interferometric autocorrelator.

The experimental arrangement used for the HHG is schematically shown in Fig. 11. The laser beam was focused with a silver-coated spherical mirror (focal length 20 cm) through an 0.3-mm-thick fused-silica window into a vacuum chamber containing the target at focus. The focal region was imaged onto a CCD camera. The estimated $1/e^2$ beam diameter were 50 and 70 μm in the vertical and horizontal direction, respectively. The slight ellipticity is caused by the off-axis focusing geometry using a spherical mirror. For a typical pulse energy of 0.3–0.4 mJ impinging the target, the on-axis peak intensity is estimated as $4\text{--}5 \times 10^{15}$ W/cm² on target. The target itself is formed by a 1-cm-long thin nickel tube with an inner diameter of 0.6 mm and a wall thickness of 0.05 mm. To minimize the interaction length and the gas load, the tube was squeezed to a residual inner diameter of 30 μm and its end was sealed. The holes in the tube walls in the squeezed region were bored by the laser itself. The tube was continuously backed with helium or some other noble gas with pressures up to 5 bar. To avoid reabsorption of the generated radiation in the interaction chamber the pressure

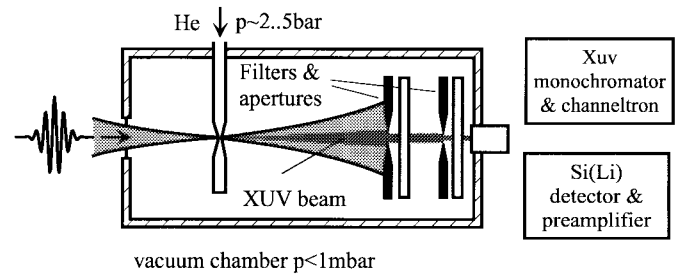


Fig. 11. Schematic of the experimental setup for measuring the high-harmonic XUV spectrum emitted by gas targets exposed to femtosecond pulses.

was kept below 1 mbar employing a root pump. From the pumping speed and the background pressure we were able to estimate the gas flow out of the target. Gas flow, target configuration, and background pressure [68] then determine uniquely the pressure in the interaction region. For a backing pressure of 5 bar, we estimated the average pressure in the interaction region as ≈ 500 mbar.

For wavelength-dispersive spectral analysis, the XUV radiation emerging from the target was passed into a 1-m grazing-incidence monochromator (Model 248/310G, McPherson Inc.) [4]. The monochromator was separated from the target chamber by a circular aperture of 1-mm diameter and evacuated by a turbo pump. This differential pumping scheme allowed the residual pressure to be reduced below 10^{-4} mbar in the monochromator, which was required by our single-channel electron multiplier detector (uncoated channeltron, Model 4175 G, Galileo). The monochromator was equipped with a 300-grooves-per-mm platinum-coated grating. The output of the detector was collected by a high-dynamic-range lock-in amplifier, which was synchronized by the laser pulse train. Alternatively, energy dispersive X-ray spectrometry (EDX) was employed for high-dynamic-range detection of X-rays with photon energies >170 eV [52]. To this end, the monochromator was replaced by a lithium-drifted silicon [Si(Li)] crystal detector cooled to 77 K. In this case, the X-ray beam must be strongly attenuated to make sure that no more than 1 X-ray photon hits the detector simultaneously. The impinging X-ray photon generates electron-hole pairs, whose number is proportional to the photon energy. The detector signal is preamplified and processed in a multichannel pulse height analyzer, yielding the photon energy spectrum of the emitted X-rays.

First, the HHG spectra for different noble gases were investigated using the wavelength-dispersive system. The entrance and exit slit width of the monochromator were fixed at 50 μm implying a resolution of 0.06 nm at 100 nm and 0.02 nm at 10 nm. The entrance slit and the aperture in front of the monochromator located 50 cm downstream of the target blocks an increasing part of the XUV signal for increasing wavelength because of the wavelength-dependent beam size. Correction for these two effects is expected to increase the spectral intensity of the long wavelength components by an order of magnitude in comparison to the short one. According to the information provided by the manufacturer the spectral response of the detector is fairly flat in the wavelength range

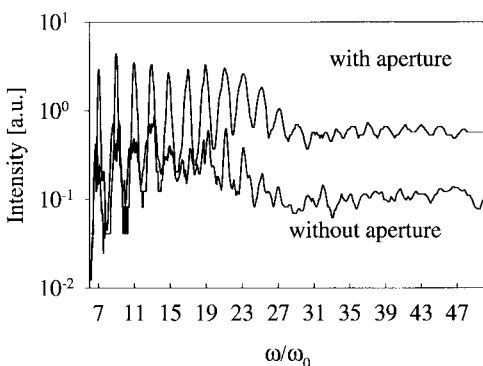


Fig. 12. Uncorrected spectrum of XUV radiation emerging from argon at a backing pressure of 0.5 bar. The upper curve was recorded after putting an aperture with a diameter of 5 mm into the laser beam prior to the focusing mirror. The beam diameter prior to the aperture was ≈ 7 mm.

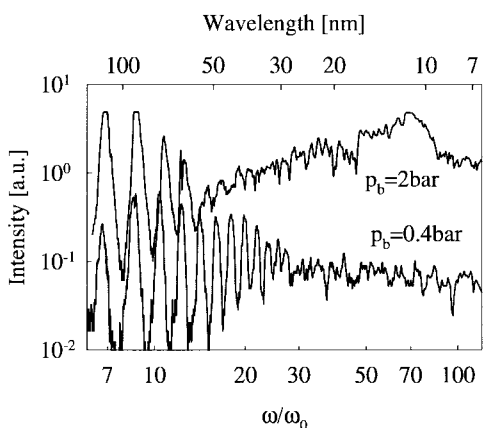


Fig. 13. Uncorrected spectrum of XUV radiation emitted by neon with a backing pressure of 0.5 and 2 bar.

of interest. In the absence of reliable information about the wavelength dependence of the grating efficiency the XUV spectra presented below have not been corrected for the spectrometer response.

The measured spectra for argon and neon are shown in Figs. 12 and 13. In these experiments, the pulse energy on target was about $300 \mu\text{J}$ and $f/30$ focusing yielded an estimated on-axis peak intensity of $\approx 4 \times 10^{15} \text{ W/cm}^2$. The radiation spectrum of argon for a backing pressure of 0.5 bar shows well resolved discrete harmonics up to the 31st order. Above this frequency the harmonics merge to a continuum. Reducing the pulse energy by $\approx 50\%$ by aperturing the laser beam before the focusing mirror resulted in a shift of the transition from discrete harmonics to continuum to the 43rd order. On the other hand, increasing the backing pressure up to 1 bar shifted the border of the continuum toward longer wavelengths. We repeated these measurements with neon at backing pressures of 0.4 and 2 bar, and observed a qualitatively similar behavior. These observations along with an increasing blue shift of the discrete harmonics with increasing backing pressure points to a nonnegligible role of plasma-induced SPM in these media [69]–[71].

Theory as well as previous experiments suggest that XUV radiation with the highest possible photon energy can be expected from helium. This is because helium has the highest

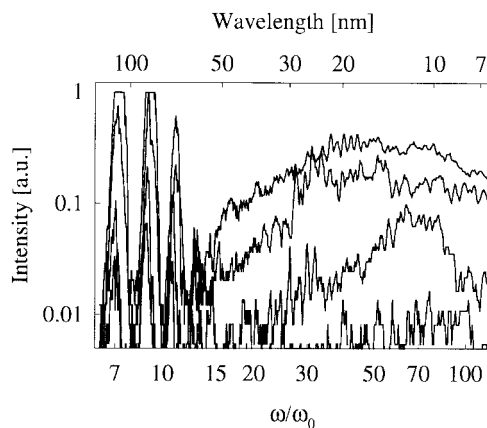


Fig. 14. Uncorrected spectra of XUV emission from helium for backing pressures of 1, 2, 4, and 5 bar. The spectral intensity increases with increasing pressure.

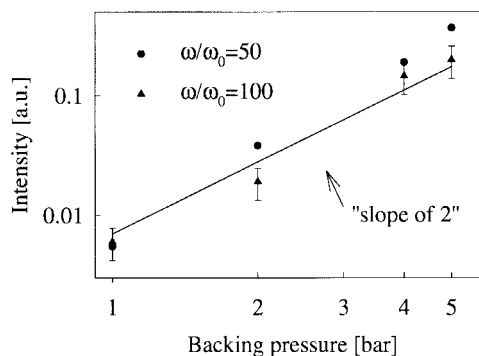


Fig. 15. Pressure dependence of the XUV intensity for different harmonic orders in helium.

ionization potential (24.4 eV) among all noble gases and hence can be exposed to the highest intensities before ionizing. The experiments reported below were performed using helium as the target material. Fig. 14 plots a wide-band scan extending from 100 to 7 nm. The spectral behavior differs from that observed with argon or neon. Discrete harmonics appear only up to the 13th order. In contrast with argon or neon, the number of discrete harmonics appears to be constant in helium up to backing pressures of 5 bar. To check whether the observed XUV radiation results from a coherent generation process (rather than, e.g., incoherent plasma emission), we measured the XUV signal as a function of the backing pressure. Fig. 15 depicts the variation of XUV spectral intensity with pressure at two different frequencies. The quadratic pressure dependence evaluated provides clear evidence for the coherent nature of the XUV emission from the ensemble [72].

The high-energy end of the continuum can not be accessed from the previous measurements because of the rapidly increasing amount of stray XUV light leaking through as the zeroth order is approached. The leakage becomes dominant for wavelengths below 7 nm. For a detailed investigation of the spectrum below 10 nm it is necessary to suppress the scatter from the central image (zeroth order) of the monochromator. To this end, a 100-nm silver foil, fixed on an electroformed nickel mesh (open area 80%) was placed in front of the entrance slit. The filter has a nearly constant transmission

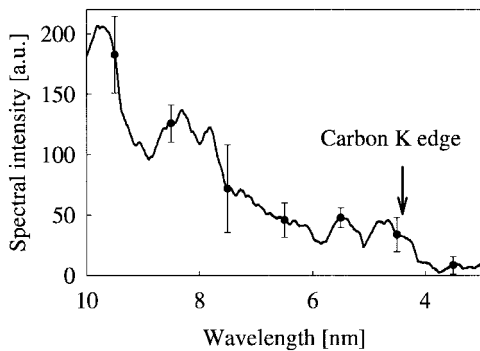


Fig. 16. Short-wavelength end of the XUV continuum emitted by the helium jet, as transmitted by a 100-nm-thick silver foil. The spectrum is the average of three scans. The error bars give the standard deviation of the signal at selected wavelengths averaged over several seconds. The spectral components at $\lambda > 10$ nm are damped by the silver foil.

of about 50% in the wavelength range of 3–10 nm and blocks radiation with wavelengths greater than 10 nm. The short wavelength tail of the XUV continuum was obtained by averaging over three scans and is shown in Fig. 16. To clarify whether the observed structure of the spectrum is real or caused by fluctuations of the experimental parameters, we measured the signal for fixed wavelengths over several seconds. The rms deviations are displayed as error bars in Fig. 16. In the wavelength range of 4.2–4.4 nm, the detector signal exceeds the noise floor by a factor of ≈ 500 . The noise floor is defined as the signal level with either the gas flow or the laser blocked. Further evidence for the signal originating from coherent XUV radiation rather than incoherent plasma emission can be gained from the fact that no measurable signal was observed after replacing helium with argon, although the ionization potential of argon is much lower than for helium, implying a much higher plasma density for argon. Systematic tests also ruled out the possibility that the tube wall contributes to the measured signal. Last but not least, increasing the pump pulse duration at constant pulse energy makes the short-wavelength tail of the spectrum to retreat to longer wavelengths, as expected from the theoretical considerations on HHG in the previous section.

In order to verify the calibration of our monochromator and provide additional evidence for the emergence of water-window radiation from the He target, we replaced the silver foil by a pair of 900-nm-thick Mylar foils ($C_{10}H_8O_4$). At 4.37 nm, the carbon K-edge, this filter provides an absorption contrast of $>10^3$. The measured spectrum shown in Fig. 17 exhibits a sharp cutoff at 4.37 nm, providing conclusive evidence for water window radiation. The signal contrast at the carbon K-edge of $>3 \times 10^3$ was limited by the noise floor of our detection apparatus. Drawing on data provided by the manufacturers of the spectrograph and the detector, a conservative estimate yields some 100 X-ray photons generated by a single laser pulse within a 1% bandwidth at the carbon K-edge.

The signal shown in Fig. 16 is found to exceed the detection limit by more than an order of magnitude down to 3 nm. At these short wavelengths, however, the exit slit is very close to the zeroth order of the diffraction grating. Therefore, some stray light contribution to the signal can not be ruled out. In

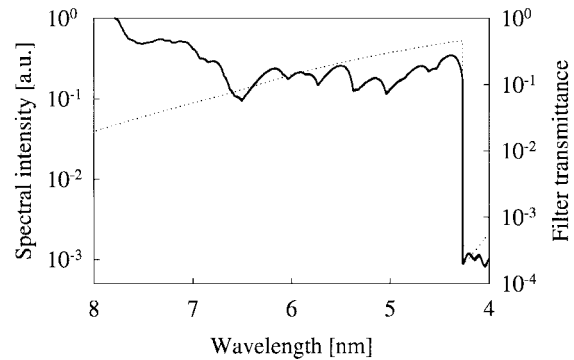


Fig. 17. Short-wavelength end of the XUV spectrum as transmitted by a 1.8- μ m-thick mylar foil (solid line) and transmittance of the foil (dotted line).

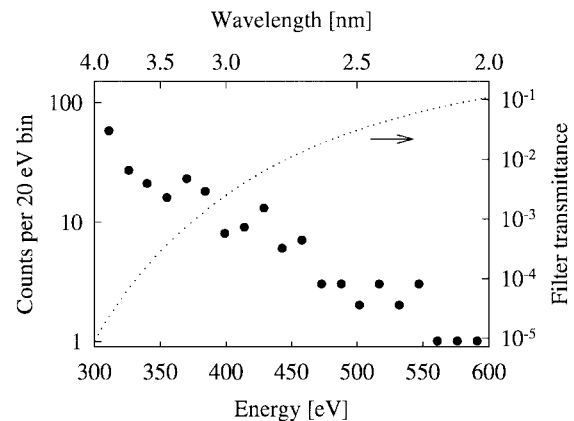


Fig. 18. High-energy end of the XUV spectrum for 7-fs pump pulses (9×10^5 shots) transmitted through 400-nm boron and 200-nm aluminum (dotted line). The photon energy spectrum has been obtained with the EDX system.

order to get around this problem, the short wavelength end of the spectrum was also studied with an energy dispersive system (ZMAX, NORAN Instruments) [52]. The lithium-drifted silicon detector is able to reliably identify only single X-ray photons with an energy greater than 170 eV. Yet, the flux at low photon energies must be suppressed with appropriate filters to avoid pile-ups, i.e., the simultaneous detection of two or more photons, which would falsify the photon energy spectrum. For safe avoidance of pile-ups the number of counts per laser shot had been reduced far below unity (≈ 0.01). After the appropriate filtering the system yielded reliable information of the photon energy spectrum of the emitted X-ray radiation. In order to gain access to the spectral region beyond 300 eV we used a 200-nm aluminum and a 400-nm boron foil to suppress low-energy radiation. With this filter combination and a count/shot probability as low as 0.5% pile-ups could be safely eliminated. The transmitted X-ray spectrum along with the filter transmittance (dashed line) is shown in Fig. 18. Fig. 18 reveals that the XUV spectrum extends beyond 500 eV, i.e., to the short-wavelength edge of the water window at 2.3 nm, the K-edge of oxygen.

The observed shape of the high energy end of the spectra strongly deviates from that of the single atom response, as shown in Fig. 6. The radiation spectrum of a He atom driven by 5-fs pulses exhibits a broad plateau of nearly constant

intensity. For a peak laser intensity of 3×10^{15} W/cm², which finds a large fraction of the He atoms in their ground state for a 5-fs pulse as revealed by Fig. 1, (3) predicts this plateau to extend to a wavelength of around 2 nm. The striking discrepancy between the predicted plateau and the rapid roll off of the XUV spectral intensity for decreasing wavelengths (see Figs. 16 and 18) is attributed to a rapidly decreasing coherence length for increasing XUV frequency in our high-pressure target [6], [52]. The dephasing is caused by an accumulating phase error due to plasma dispersion and wave front curvature, both of which rapidly increase in importance with decreasing wavelengths. For our focusing geometry, the accumulating phase error introduced by the curvature of the fundamental wave front limits coherent accumulation of XUV radiation to an interaction length (geometric coherence length) on the order of 5–10 μm for wavelengths in the water window [61]. The high pressure used in our experiments is dictated by the short geometric coherence length associated with tight focusing of the pump laser, which was necessary to achieve the required peak intensities with our present source. Roughly, optimum signal can be expected at a pressure which makes the coherence length determined by plasma dispersion only approximately equal to the geometric coherence length. The role of plasma dispersion was extensively analyzed in the previous section. According to our computer simulations (see Fig. 9) the respective coherence length for radiation around the carbon K-edge is on the order of 5 μm for a target pressure of 0.5 bar. This compares well with the estimated geometric coherence length for the same XUV wavelength region and explains why we had to rely on the high pressures for maximum XUV emission in the water window in our experiments. Because the total interaction length, i.e., target thickness could not be confined to a few micrometers (rather it was estimated as 100–150 μm), the increasing coherence length for increasing wavelength resulted in a rapidly increasing spectral intensity. We expect that the availability of somewhat higher pulse energies (of 1–3 mJ) will allow a significant enhancement of the X-ray flux in the water window owing to the more gentle focusing and associated more relaxed conditions for optimizing coherence growth of the emitted radiation.

For practical applications of this X-ray source the spatial coherence is of great interest. To acquire some information about the spatial properties of the X-rays, a knife edge was transversely scanned across the beam. The transmitted power as a function of the knife edge position was recorded [73] for different wavelengths. The knife edge was positioned 29 cm downstream of the helium source. In Fig. 19, the transmitted power is shown for wavelengths at 4.4 and 10 nm. The diagram also depicts Gaussian fits to the measured data (dashed line), which yielded a $1/e^2$ -diameter of 480 and 180 μm at a wavelength of 10 and 4.4 nm, respectively. The corresponding beam divergence was estimated as <1 mrad and <0.5 mrad at 10 and 4.4 nm, respectively. Taking into account the transverse size of the XUV source, from these measurements we conclude that the emitted X-ray beam is within a factor of three diffraction limited (i.e., can be characterized with $M^2 < 3$ [74]). Assuming an X-ray beam

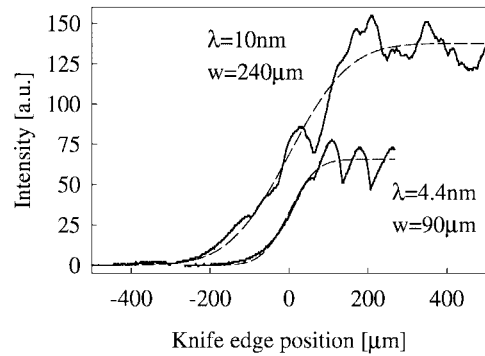


Fig. 19. Transmitted X-ray signal as a function of the position of a knife edge scanning transversely across the beam 29 cm downstream of the He target at two different wavelengths. The dashed lines depict Gaussian fits to the measured profiles.

diameter of 25 μm at the beam waist (in the source), we estimate the (time-averaged) brightness of the presented source at the carbon K-edge within a 1% bandwidth as 5×10^8 photons mm^{-2} mrad^{-2} s^{-1} . An upgrade of the laser driver to a pump pulse energy of several millijoules and further optimization of the XUV generation process is expected to increase both the peak and the average brightness of the present source by some two orders of magnitude. The former should then allow focusing the beam to peak intensities as high as 10^{15} W/cm² in the sub-10-nm wavelength range and open the way toward an extension of nonlinear optics into the X-ray regime [44], [75]. The latter should allow focusing the output to average intensities sufficiently high for permitting biological microscopy [76] and holography [77], [89] in the water window.

V. TOWARDS THE GENERATION OF SINGLE ATTOSECOND XUV PULSES

In this section, we shall briefly address the temporal evolution of the coherent XUV radiation emitted at wavelengths below 10 nm and the challenges the predicted temporal behavior presents to the experimenter. The results of simulations presented in Section III suggest that the short-wavelength end of the X-ray spectrum emerging from helium driven by a 5-fs laser pulse is emitted in a single subfemtosecond burst. Transmitting the spectral components in the range of $240 < \omega/\omega_0 < 280$ (corresponding to wavelengths between 2.7 and 3.3 nm) through an appropriate filter, a single pulse with a duration of ≈ 100 as can be expected.

The theoretical analysis underlines the crucial role of propagation effects in selecting a clean single pulse for sub-10-fs laser drivers and suggests that the relative carrier phase ψ_0 of the laser pulse described by the electric field $E_t(t) = A_t(t) \exp(-i\omega_0 t + i\psi_0)$ plays an important role for the generation and control of single XUV attosecond pulses. In fact, numerical experiments clearly revealed that the evolution of the (filtered) instantaneous X-ray intensity on an attosecond time scale is a sensitive function of ψ_0 . Both the peak intensity and the timing (with respect to the laser pulse) varies with ψ_0 . As a consequence, the relative carrier phase (henceforth briefly: carrier phase) of the quasi-single-cycle laser

pulse needs to be controlled for stable and fully controllable generation of single-attosecond XUV pulses. Unfortunately, CW mode-locked lasers, the primary sources of ultrashort pulses, do not produce pulses with a constant carrier phase. Recent experiments performed with a sub-10-fs Ti:sapphire laser revealed that even under optimum conditions the carrier phase is subject to rapid variations in the emitted pulse train [67]. Stabilization of the carrier phase calls for a process that yields a physical measurable which is sensitive to the phase. Our investigations indicate that phase sensitive effects can be explored in the strong-field regime of nonlinear optics, where the fast-oscillating electric field, rather than its slowly varying envelope governs light-matter interactions. Until recently, the intensity levels directly achievable with a CW mode-locked laser did not allow accessing the strong-field regime. Recent advances in sub-10-fs Ti:sapphire oscillator technology permitted focusing the mode-locked laser pulses to intensities higher than 5×10^{13} W/cm² [85]. These intensities should be sufficiently high for inducing photoemission in the tunneling regime from a gold photocathode. This process would yield a photocurrent (averaged over the pulse repetition time) which is dependent on the carrier phase in the sub-10-fs regime [78]. This ψ_0 -dependent signal could then be coupled into a feedback servo loop for stabilizing the carrier phase as proposed in [67]. This route represents a promising approach to realizing a phase-stabilized sub-10-fs pump source for coherent XUV generation.

Another issue that needs to be addressed is the spatial variation of the emitted XUV radiation. It is evident that the temporal evolution of the generated X-rays is subject to a strong spatial variation if the intensity of the driving laser field exhibits a radial variation on target. The adverse consequences include among others a spatially varying timing of the single attosecond pulse with a selected center frequency with respect to the peak of the laser pulse. As a consequence, focusing of the X-ray pulse would result in a pulse broadening up to several femtoseconds. This drawback can be eliminated by realizing a nearly flat-top intensity profile on target. This can, among others, be achieved by placing a hard aperture of suitable diameter in the collimated laser beam and imaging the aperture plane onto the target. The next question that arises is whether appropriate filters can be found which fulfill a couple of requirements: they 1) have to efficiently suppress longer-wavelength radiation with a sufficiently steep cut off and 2) may not cause significant dispersive broadening of the transmitted pulse. It can be shown, that a 200-nm aluminum filter in combination with a 200-nm titanium filter meet the above requirements.

Last but not least, once the attosecond pulses can be reliably produced they need to be characterized temporally before they can be used for applications. Recently, the ninth harmonic of a femtosecond Ti:sapphire laser was measured by autocorrelation [79]. The pulses were recombined in a helium jet and generated He⁺ ions by two-photon ionization. In the absence of neutral atoms with correspondingly high ionization potential, this technique can not be extended to the wavelength range of around 10 nm or shorter. However, a vacancy could be produced in the K-shell of some light element

(e.g., O, N, C, B, Be) by two-photon absorption, resulting in fluorescence at photon energies approximately equal to twice the absorbed photon energy. Unfortunately, the two-photon absorption cross section scales with the fourth power of the wavelength and hence, is much smaller than around 100 nm [80]. As a consequence, tight focusing and the use of a sensitive technique for detecting the two-photon-absorption-induced fluorescence will be inevitable. Estimations [80] show that the contemplated upgrade of the sub-10-fs laser driver along with the use of a state-of-the-art toroidal focusing mirror might result in a fluorescence yield that can be detected by a single-photon-counting EDX system. This would not only permit attosecond pulse measurement but also constitute, to the best of our knowledge, the first nonlinear optical experiment performed with X-rays. Finally, it should be noted that a corollary of single attosecond pulse generation will be the complete disappearance of harmonic structure in the XUV spectrum. This may be important for such spectroscopy applications as X-ray fine structure absorption spectroscopy (EXAFS) in the vicinity of the carbon K-edge.

VI. SUMMARY

The above applications clearly indicate that the significance of intense few-cycle laser pulses is likely to go well beyond the frontiers of physical sciences. A laboratory-scale source of coherent X-rays in the water window will undoubtedly make a major impact on high-contrast live biological X-ray microscopy [76] and holography [77], [89]. Further optimization of the above demonstrated 5-fs-pulse-driven harmonic generator (e.g., by the implementation of quasi-phase matching) may allow the development of the first laboratory tool suitable for *in vivo* microscopy of living organisms with a resolution, which approaches the virus, DNA, and RNA scales. The predicted "concentration" of the high-energy XUV photons in a *single* burst of attosecond duration may not only extend nonlinear optics into the X-ray regime and allow studying the dynamics of bound electrons, but also provide a tool for studying chemical reactions and wave packet dynamics on a previously inaccessible time scale. Polarization control of the 5-fs infrared driver pulse allows the emission of a subfemtosecond electron burst with well-determined energy distribution [43]. The possibility of injecting an intense subfemtosecond electron burst into a plasma in a controlled manner is likely to benefit the development of laser-driven particle accelerators [81], [82] as well as electron-pumped X-ray lasers in the keV regime [39]. Nevertheless, at present we are just at the stage of exploring the new possibilities and phenomena, and a number of technical barriers are left to be overcome before these exciting prospects can materialize.

ACKNOWLEDGMENT

The contributions by S. Sartania, M. Lenzner, Z. Cheng, R. Koppitsch, P. Wobrauschek, and C. Streltsov to the above experiments are gratefully acknowledged. The authors would also like to thank A. J. Schmidt for his encouragement.

REFERENCES

- [1] S. Sartania, Z. Cheng, M. Lenzner, G. Tempea, C. Spielmann, F. Krausz, and K. Ferencz, "Generation of 0.1-TW 5-fs optical pulses at a 1-kHz repetition rate," *Opt. Lett.*, vol. 22, pp. 1562–1564, 1997.
- [2] D. Attwood, K. Halbach, and K.-J. Kim, "Tunable coherent X-rays," *Science*, vol. 228, pp. 1265–1272, 1985.
- [3] B. J. MacGowan, S. Maxon, L. B. Da Silva, D. J. Fields, C. J. Keane, D. L. Matthews, A. L. Osterheld, J. H. Scofield, A. Shimkaveg, and G. F. Stone, "Demonstration of X-ray amplifiers near the carbon K edge," *Phys. Rev. Lett.*, vol. 65, pp. 420–423, 1990.
- [4] C. Spielmann, N. H. Burnett, S. Sartania, R. Koppitsch, M. Schnürer, C. Kan, M. Lenzner, P. Wobrauschek, and F. Krausz, "Generation of coherent X-rays in the water window using 5-fs laser pulses," *Science*, vol. 278, pp. 661–663, 1997.
- [5] Z. Chang, A. Rundquist, H. Wang, M. Murnane, and H. C. Kapteyn, "Generation of coherent soft X-rays at 2.7 nm using high harmonics," *Phys. Rev. Lett.*, vol. 79, pp. 2967–2971, 1997.
- [6] C. Kan, N. H. Burnett, C. Capjack, and R. Rankin, "Coherent XUV generation from gases ionized by several cycle optical pulses," *Phys. Rev. Lett.*, vol. 79, pp. 2971–2974, 1997.
- [7] P. F. Moulton, "Spectroscopic and laser characteristics of Ti:Al₂O₃," *J. Opt. Soc. Amer. B*, vol. 3, pp. 125–133, 1986.
- [8] D. E. Spence, P. N. Kean, and W. Sibbett, "60-fsec pulse generation from a self-modelocked Ti:sapphire laser," *Opt. Lett.*, vol. 16, pp. 42–44, 1991.
- [9] R. Szipöcs, K. Ferencz, C. Spielmann, and F. Krausz, "Chirped multilayer coatings for broadband dispersion control in femtosecond lasers," *Opt. Lett.*, vol. 19, pp. 201–203, 1994.
- [10] A. Stingl, M. Lenzner, C. Spielmann, F. Krausz, and R. Szipöcs, "Sub-10-femtosecond, mirror-dispersion-controlled Ti:sapphire laser," *Opt. Lett.*, vol. 20, pp. 602–604, 1995.
- [11] L. Xu, G. Tempea, A. Poppe, M. Lenzner, C. Spielmann, F. Krausz, A. Stingl, and K. Ferencz, "High power sub-10fs Ti:sapphire oscillators," *Appl. Phys. B*, vol. 65, pp. 151–159, 1997.
- [12] I. Jung, F. X. Kärtner, N. Matuschek, D. H. Sutter, F. Morier-Genoud, G. Zhang, U. Keller, V. Scheuer, M. Tilsch, and T. Tschudi, "Self-starting 6.5 fs pulses from a Ti:sapphire laser," *Opt. Lett.*, vol. 22, pp. 1009–1011, 1997.
- [13] D. Strickland and G. Mourou, "Compression of amplified chirped optical pulses," *Opt. Commun.*, vol. 56, pp. 219–221, 1985.
- [14] J. Squier, F. Salin, G. Mourou, and D. Harter, "100-fs pulse generation and amplification in Ti:Al₂O₃," *Opt. Lett.*, vol. 16, pp. 324–326, 1991.
- [15] J. D. Kmetec, J. J. Macklin, and J. F. Young, "0.5TW, 125-fs Ti:sapphire laser," *Opt. Lett.*, vol. 16, pp. 1001–1003, 1991.
- [16] A. Sullivan, H. Hamster, H. C. Kapteyn, S. Gordon, W. White, H. Nathel, R. J. Blair, and R. W. Falcone, "Multiterawatt, 100-fs laser," *Opt. Lett.*, vol. 16, pp. 1406–1408, 1991.
- [17] K. Yamakawa, H. Siraga, Y. Kato, and C. P. J. Barty, "Prepuls-free 30-TW, 1 ps Nd: Glass laser," *Opt. Lett.*, vol. 16, pp. 1593–1595, 1991.
- [18] T. B. Norris, "Femtosecond pulse amplification at 250 kHz with a Ti:sapphire regenerative amplifier and application to continuum generation," *Opt. Lett.*, vol. 17, pp. 1009–1011, 1992.
- [19] J. V. Rudd, G. Korn, S. Kane, J. Squier, G. Mourou, and P. Bado, "Chirped-pulse amplification of 55-fs pulses at a 1-kHz repetition rate in a Ti:Al₂O₃ regenerative amplifier," *Opt. Lett.*, vol. 18, pp. 2044–2046, 1993.
- [20] J. P. Zhou, C. P. Huang, C. Shi, H. C. Kapteyn, and M. M. Murnane, "Generation of 21-fs millijoule-energy pulses by use of Ti:sapphire," *Opt. Lett.*, vol. 19, pp. 126–128, 1994.
- [21] C. P. J. Barty, C. L. Gordon, III, and B. E. Lemoff, "Multiterawatt 30-fs Ti:sapphire laser system," *Opt. Lett.*, vol. 19, pp. 1442–1444, 1994.
- [22] J. P. Zhou, C. P. Huang, M. M. Murnane, and H. C. Kapteyn, "Amplification of 26-fs 2-TW pulses near the gain-narrowing limit in Ti:sapphire," *Opt. Lett.*, vol. 20, pp. 64–66, 1995.
- [23] M. Lenzner, C. Spielmann, E. Wintner, F. Krausz, and A. J. Schmidt, "Sub-20 fs, kilohertz-repetition-rate Ti:sapphire amplifier," *Opt. Lett.*, vol. 20, pp. 1397–1399, 1995.
- [24] S. Backus, J. Peatross, C. P. Huang, M. M. Murnane, and H. C. Kapteyn, "Ti:sapphire amplifier producing millijoule-level 21-fs pulses at 1 kHz," *Opt. Lett.*, vol. 20, pp. 2000–2002, 1995.
- [25] C. P. J. Barty, T. Guo, C. Le Blanc, F. Raksi, C. Rose-Petruck, J. Squier, K. R. Wilson, V. V. Yakovlev, and K. Yamakawa, "Generation of 18-fs multiterawatt pulses by regenerative pulse shaping and chirped-pulse amplification," *Opt. Lett.*, vol. 21, pp. 668–670, 1996.
- [26] J. P. Chambaret, C. Le Blanc, G. Cheriaux, P. Curley, G. Darpentigny, P. Rousseau, G. Hamoniaux, A. Antonetti, and F. Salin, "Generation of 25-TW, 32-fs pulses at 10 Hz," *Opt. Lett.*, vol. 21, pp. 1921–1923, 1996.
- [27] S. Backus, C. G. Durfee, III, G. Mourou, H. C. Kapteyn, and M. M. Murnane, "0.2 TW laser system at 1 kHz," *Opt. Lett.*, vol. 22, pp. 1256–1258, 1997.
- [28] M. Nisoli, S. De Silvestri, and O. Svelto, "Generation of high energy 10 fs pulses by a new pulse compression technique," *Appl. Phys. Lett.*, vol. 68, pp. 2793–2795, 1996.
- [29] A. Baltuska, Z. Wei, M. S. Pshenichnikov, and D. A. Wiersma, "Optical pulse compression to 5fs at a 1-MHz repetition rate," *Opt. Lett.*, vol. 22, pp. 102–104, 1997.
- [30] M. Nisoli, S. Stagira, S. De Silvestri, O. Svelto, S. Sartania, Z. Cheng, G. Tempea, C. Spielmann, and F. Krausz, "Toward a terawatt-scale sub-10fs laser technology," this issue, pp. 414–420.
- [31] M. Nisoli, S. De Silvestri, O. Svelto, R. Szipöcs, K. Ferencz, C. Spielmann, S. Sartania, and F. Krausz, "Compression of high-energy laser pulses below 5 fs," *Opt. Lett.*, vol. 22, pp. 522–524, 1997.
- [32] G. Tempea, F. Krausz, C. Spielmann, and K. Ferencz, "Dispersion control over 150 THz with chirped dielectric mirrors," this issue, pp. 193–196.
- [33] L. V. Keldysh, "Ionization in the field of a strong electromagnetic wave," *Sov. Phys. JETP*, vol. 20, pp. 1307–1314, 1965.
- [34] M. V. Ammosov, N. B. Delone, and V. P. Krainov, "Tunneling ionization of complex atoms and atomic ions by an alternating electromagnetic field," *Sov. Phys. JETP*, vol. 64, pp. 1191–1194, 1986.
- [35] V. P. Krainov, "Ionization rates and energy and angular distribution at the barrier-suppression ionization of complex atoms and atomic units," *J. Opt. Soc. Amer. B*, vol. 14, pp. 425–431, 1997.
- [36] A. L'Huillier and P. Balcou, "High-order harmonic generation in rare gases with a 1-ps 1053-nm laser," *Phys. Rev. Lett.*, vol. 70, pp. 774–777, 1993.
- [37] J. J. Macklin, J. D. Kmetec, and C. L. Gordon, III, "High-order harmonic generation using intense femtosecond pulses," *Phys. Rev. Lett.*, vol. 70, pp. 766–769, 1993.
- [38] B. E. Lemoff, C. P. J. Barty, and S. E. Harris, "Femtosecond-pulse-driven, electron excited XUV lasers in eight-times-ionized noble gases," *Opt. Lett.*, vol. 19, pp. 569–571, 1994.
- [39] C. P. J. Barty, T. Guo, C. Le Blanc, F. Raksi, C. G. Rose-Petruck, J. A. Squier, B. C. Walker, K. R. Wilson, V. V. Yakovlev, and K. Yamakawa, "Sub-20-fs multiterawatt lasers and X-ray applications," in *Proc. 5th Int. Conf. X-ray Lasers*, S. Svaneberg and C. G. Wahlström, Eds. Bristol, U.K.: Inst. of Phys., 1996, pp. 282–288.
- [40] P. B. Corkum, N. H. Burnett, and F. Brunel, "Above-threshold ionization in the long-wavelength limit," *Phys. Rev. Lett.*, vol. 62, pp. 1259–1262, 1989.
- [41] P. B. Corkum, "Plasma perspective on strong-field multiphoton ionization," *Phys. Rev. Lett.*, vol. 71, pp. 1994–1997, 1993.
- [42] K. C. Kulander, K. J. Schafer, and J. L. Krause, "Dynamics of short-pulse excitation, ionization and harmonic conversion," in *Proc. Workshop Super Intense Laser Atom Physics (SILAP III)*, B. Pirauk, Ed. New York: Plenum, 1993, vol. 316, p. 95.
- [43] P. B. Corkum, N. H. Burnett, and M. Yu. Ivanov, "Subfemtosecond pulses," *Opt. Lett.*, vol. 19, pp. 1870–1872, 1994.
- [44] P. Antoine, A. L'Huillier, and M. Lewenstein, "Attosecond pulse trains using high-order harmonics," *Phys. Rev. Lett.*, vol. 77, pp. 1234–1237, 1996.
- [45] K. J. Schafer and K. C. Kulander, "High harmonic generation from ultrafast pump lasers," *Phys. Rev. Lett.*, vol. 78, pp. 638–641, 1997.
- [46] I. P. Christov, M. M. Murnane, and H. C. Kapteyn, "High harmonic generation of attosecond pulses in the 'single-cycle' regime," *Phys. Rev. Lett.*, vol. 78, pp. 1251–1254, 1997.
- [47] N. H. Burnett and P. B. Corkum, "Cold-plasma production for recombination extreme-ultraviolet lasers by optical-field-induced ionization," *J. Opt. Soc. Amer. B*, vol. 6, pp. 1195–1199, 1989.
- [48] S. M. Hooker and S. E. Harris, "Femtosecond-pulse-driven electron-excited extreme-ultraviolet lasers in Be-like ions," *Opt. Lett.*, vol. 20, pp. 1994–1996, 1995.
- [49] P. Kalman and T. Brabec, "Generation of coherent hard X-ray radiation in crystalline solids by high-intensity femtosecond laser pulses," *Phys. Rev. A*, vol. 52, pp. R21–R24, 1995.
- [50] ———, "Evolution of coherent hard X-ray radiation in crystalline solids by high-intensity femtosecond laser pulses," *Phys. Rev. A*, vol. 53, pp. 627–629, 1996.
- [51] M. Lewenstein, P. Balcou, M. Yu. Ivanov, A. L'Huillier, and P. B. Corkum, "Theory of high-harmonic generation by low frequency laser fields," *Phys. Rev. A*, vol. 49, pp. 2117–2132, 1994.
- [52] M. Schnürer, C. Spielmann, P. Wobrauschek, C. Strelhi, N. H. Burnett, C. Kan, K. Ferencz, R. Koppitsch, Z. Cheng, and F. Krausz, "Coherent 0.5-keV X-ray emission from helium driven by a sub-10 fs laser," *Phys. Rev. Lett.*, vol. 80, pp. 3236–3238, 1998.

- [53] D. Du, X. Liu, G. Korn, J. Squier, and G. Mourou, "Laser-induced breakdown by impact ionization in SiO₂ with pulse widths from 7ns to 150fs," *Appl. Phys. Lett.*, vol. 64, pp. 3071–3073, 1994.
- [54] B. C. Stuart, M. D. Feit, A. M. Rubenchik, B. W. Shore, and M. D. Perry, "Laser-induced damage in dielectrics with nanosecond to picosecond pulses," *Phys. Rev. Lett.*, vol. 74, pp. 2248–2251, 1995.
- [55] T. Seidemann, M. Yu. Ivanov, and P. B. Corkum, "Role of electron localization in intense-field molecular ionization," *Phys. Rev. Lett.*, vol. 75, pp. 2819–2822, 1995.
- [56] S. Chelkowski, A. Conjusteau, T. Zuo, and A. D. Bandrauk, "Dissociative ionization of H₂⁺ in an intense laser field: Charge-resonance-enhanced ionization, Coulomb explosion, and harmonic generation at 600 nm," *Phys. Rev. A*, vol. 54, pp. 3235–3244, 1996.
- [57] S. C. Rae and K. Burnett, "Possible production of cold plasma through optical-field-induced ionization," *Phys. Rev. A*, vol. 46, pp. 2077–2083, 1992.
- [58] H. A. Bethe and E. E. Salpeter, *Quantum Mechanics of One- and Two-Electron Atoms*. New York: Plenum, 1977.
- [59] J. R. Oppenheimer, "Three notes on the quantum theory of aperiodic effects," *Phys. Rev.*, vol. 13, pp. 66–81, 1928.
- [60] L. D. Landau and E. M. Lifshitz, *Quantum Mechanics*, 2nd ed. New York: Pergamon, 1965, p. 276.
- [61] A. L'Huillier, L.-A. Lompre, G. Mainfray, and C. Manus, "High-order harmonic generation in rare gases," in *Atoms in Intense Laser Fields*, M. Gavrilla, Ed. New York: Academic, 1992, pp. 139–206.
- [62] J. Zhou, J. Peatross, M. M. Murnane, H. C. Kapteyn, and I. P. Christov, "Enhanced high-harmonic generation using 25fs laser pulses," *Phys. Rev. Lett.*, vol. 76, pp. 752–755, 1996.
- [63] T. Brabec and F. Krausz, "Nonlinear optical pulse propagation in the single-cycle regime," *Phys. Rev. Lett.*, vol. 78, pp. 3282–3285, 1997.
- [64] A. L'Huillier, K. J. Schafer, and K. C. Kulander, "Theoretical aspects of intense field harmonic generation," *J. Phys. B: Atom. Mol. Phys.*, vol. 24, pp. 3315–3341, 1991.
- [65] E. Esary, G. Joyce, and P. Sprangle, "Frequency up-shifting of laser pulses by copropagating ionization fronts," *Phys. Rev. A*, vol. 44, pp. 3908–3911, 1991.
- [66] T. Ditmire, K. Kulander, J. K. Crane, H. Nguyen, and M. D. Perry, "Calculation and measurement of high-order harmonic energy yields in helium," *J. Opt. Soc. Amer. B*, vol. 13, pp. 406–411, 1996.
- [67] L. Xu, C. Spielmann, A. Poppe, T. Brabec, F. Krausz, and T. Hänsch, "Route to phase control of ultrashort light pulses," *Opt. Lett.*, vol. 21, pp. 2008–2010, 1996.
- [68] H. Zoehl and J. Kruschik, *Strömung durch Rohre und Ventile*. Vienna, Austria: Springer, 1982.
- [69] S. C. Rae, K. Burnett, and J. Cooper, "Generation and propagation of high-order harmonics in a rapidly ionizing medium," *Phys. Rev. A*, vol. 50, pp. 3438–3446, 1994.
- [70] K. Myazaki and H. Takada, "High-order harmonic generation in the tunneling regime," *Phys. Rev. A*, vol. 52, pp. 3007–3021, 1995.
- [71] C. Altucci, T. Starczewski, E. Mevel, C.-G. Wahlström, B. Carre, and A. L'Huillier, "Influence of atomic density in high-order harmonic generation," *J. Opt. Soc. Amer. B*, vol. 13, pp. 148–156, 1996.
- [72] J. Peatross and D. D. Meyerhofer, "Intensity-dependent atomic-phase effects in high-order harmonic generation," *Phys. Rev. A*, vol. 52, pp. 3976–3987, 1995.
- [73] A. E. Siegman, M. W. Sasnett, and T. F. Johnson, "Choice of clip levels for beam width measurements using knife-edge techniques," *IEEE J. Quantum Electron.*, vol. 27, pp. 1098–1091, 1991.
- [74] A. E. Siegman, "New development in laser resonators," in *Conference on Laser Resonators, SPIE*, 1990, vol. 1224, pp. 2–14.
- [75] P. Corkum, "Harmonics to quicken the pulse," *Nature*, vol. 384, pp. 118–119, 1996.
- [76] R. W. Eason, P. C. Cheng, R. Feder, A. G. Michette, R. J. Rosser, F. O'Neil, Y. Owanda, P. T. Rumsby, M. J. Shaw, and I. C. E. Turcu, "Laser X-ray microscopy," *Optica Acta*, vol. 3, pp. 501–516, 1986.
- [77] M. Howells, C. Jacobson, J. Kirz, R. Feder, K. McQuaid, and S. Rothman, "X-ray holograms at improved resolution: A study of zymogen granules," *Science*, vol. 238, pp. 514–517, 1987.
- [78] F. Krausz and C. Spielmann, private communication.
- [79] Y. Kobayashi, T. Seikikawa, Y. Nabekawa, and S. Watanabe, "27-fs XUV pulse generation by high-order harmonics," presented at the Conf. Lasers and Electro-Optics, 1997, postdeadline paper CPD4.
- [80] P. Kalman, private communication.
- [81] A. Modena, Z. Najmudin, A. E. Dangor, C. E. Clayton, K. A. Marsh, C. Joshi, V. Malka, C. B. Darrow, C. Danson, D. Neely, and F. N. Walsh, "Electron acceleration from the breaking of relativistic plasma waves," *Nature*, vol. 377, pp. 606–608, 1995.
- [82] D. Umstadter, S.-Y. Chen, A. Maksimchuk, G. Mourou, and R. Wagner, "Nonlinear optics in relativistic plasmas and laser wake field acceleration of electrons," *Science*, vol. 273, pp. 472–475, 1996.
- [83] L. Spinelli, B. Couillaud, N. Goldblatt, and D. K. Negus, "Starting and generation of sub-100fs pulses in Ti:Al₂O₃ by self focusing," in *Dig. Conf. Lasers and Electro-Optics*, Washington, DC: Opt. Soc. Amer., 1991, paper CPDP7.
- [84] U. Keller, G. W. t'Hoof, W. H. Knox, and J. E. Cunningham, "Femtosecond pulses from a continuously self-starting passively modelocked Ti:sapphire laser," *Opt. Lett.*, vol. 16, pp. 1022–1024, 1991.
- [85] L. Xu, G. Tempea, C. Spielmann, F. Krausz, A. Stingl, K. Ferencz, and S. Takano, "A CW mode-locked Ti:sapphire laser focusable to 5×10^{13} W/cm²," *Opt. Lett.*, vol. 23, May 15, 1998.
- [86] M. Nisoli, S. Stagira, S. De Silvestri, O. Svelto, S. Sartania, Z. Cheng, M. Lenzner, C. Spielmann, and F. Krausz, "A novel-high energy pulse compression system: Generation of multigigawatt sub-5 fs pulses," *Appl. Phys. B*, vol. 65, pp. 175–196, 1997.
- [87] A. M. Perelomov, V. S. Popov, and M. V. Terent'ev, "Ionization of atoms in an alternating electric field," *Sov. Phys. JETP*, vol. 23, pp. 924–934, 1966.
- [88] B. E. Lemoff, G. Y. Yin, C. L. Gordon, III, C. P. J. Barty, and S. E. Harris, "Demonstration of a 10-Hz femtosecond-pulse-driven XUV laser at 41.8 nm in Xe IX," *Phys. Rev. Lett.*, vol. 74, pp. 1574–1577, 1995.
- [89] J. E. Trebes, S. B. Brown, E. M. Campbell, D. L. Matthews, D. G. Nilson, G. F. Stone, and D. A. Whelan, "Demonstration of X-ray holography with an X-ray laser," *Science*, vol. 238, pp. 517–520, 1987.

Christian Spielmann, for photograph and biography, see this issue, p. 184.

Clarence Kan, photograph and biography not available at the time of publication.

Neal H. Burnett, photograph and biography not available at the time of publication.



Thomas Brabec born in Linz, Austria, on April 10, 1964. He received the Ph.D. degree from Vienna University of Technology, Vienna, Austria, in 1992.

In 1994, he was awarded an APART Grant. He worked as a Post-Doctoral Fellow at the NRC Canada with Dr. Paul Corkum. Currently, he is a Research Associate at the Technical University of Vienna. His research interests are the theoretical modeling of ultrashort pulse generation and propagation, and the theory of high-intensity light-matter interactions.



Michael Geissler was born in Vienna, Austria, on July 18, 1972. He received the M.Sc. degree in electrical engineering at the Vienna University of Technology, Vienna, Austria, in 1998, and currently he is working towards the Ph.D. degree.

His research focuses on the theoretical investigation of high-field light-matter interactions.



Armin Scrinzi was born in Klagenfurt, Austria, in 1959. He received the M.Sc. degree in mathematical physics in 1985 and the Ph.D. degree in theoretical physics in 1989, at the University of Vienna, Austria.

He worked as a Post-Doctoral Fellow at the University of Florida, at the Kurchatov Institute in Moscow and at the Manne Siegbahn Institute, Stockholm, Sweden. Between 1994 and 1997, he was a Fellow of the APART Program of the Austrian Academy of Sciences. His current research interests

center on mathematical and computational physics and atoms in strong external fields.



Matthias Schnürer was born in Magdeburg, Germany, in October 1956. He received the Diploma degree and the Ph.D. degree in physics on research of small gap semiconductor MOS structures at Humboldt-University in Berlin, Germany, in 1982 and 1984, respectively.

He joined the Central Institute of Optics in Berlin from 1984 to 1991 and the Max-Born-Institute in Berlin from 1992 to 1996, where he worked in the High Power Laser Departments. In 1997, he joined the Femtosecond Laser Group at the Vienna

University of Technology, Austria. His research interests include laser-plasma interaction, especially the study of laser-plasma based coherent and incoherent X-ray sources.

Ferenc Krausz (M'92), for photograph and biography, see this issue, p. 184.